NASA/TM-2014-218265

Multiscale Analysis of Structurally-Graded Microstructures Using Molecular Dynamics, Discrete Dislocation Dynamics and Continuum Crystal Plasticity

Erik Saether, Jacob D. Hochhalter, and Edward H. Glaessgen
Langley Research Center, Hampton, Virginia

Yuri Mishin
George Mason University, Fairfax, Virginia

May 2014

NASA STI Program . . . in Profile

Since its founding, NASA has been dedicated to the advancement of aeronautics and space science. The NASA scientific and technical information (STI) program plays a key part in helping NASA maintain this important role.

The NASA STI program operates under the auspices of the Agency Chief Information Officer. It collects, organizes, provides for archiving, and disseminates NASA's STI. The NASA STI program provides access to the NASA Aeronautics and Space Database and its public interface, the NASA Technical Report Server, thus providing one of the largest collections of aeronautical and space science STI in the world. Results are published in both non-NASA channels and by NASA in the NASA STI Report Series, which includes the following report types:

- TECHNICAL PUBLICATION. Reports of completed research or a major significant phase of research that present the results of NASA Programs and include extensive data or theoretical analysis. Includes compilations of significant scientific and technical data and information deemed to be of continuing reference value. NASA counterpart of peer-reviewed formal professional papers, but having less stringent limitations on manuscript length and extent of graphic presentations.

- TECHNICAL MEMORANDUM. Scientific and technical findings that are preliminary or of specialized interest, e.g., quick release reports, working papers, and bibliographies that contain minimal annotation. Does not contain extensive analysis.

- CONTRACTOR REPORT. Scientific and technical findings by NASA-sponsored contractors and grantees.

- CONFERENCE PUBLICATION. Collected papers from scientific and technical conferences, symposia, seminars, or other meetings sponsored or co-sponsored by NASA.

- SPECIAL PUBLICATION. Scientific, technical, or historical information from NASA programs, projects, and missions, often concerned with subjects having substantial public interest.

- TECHNICAL TRANSLATION. English-language translations of foreign scientific and technical material pertinent to NASA's mission.

Specialized services also include organizing and publishing research results, distributing specialized research announcements and feeds, providing information desk and personal search support, and enabling data exchange services.

For more information about the NASA STI program, see the following:

- Access the NASA STI program home page at *http://www.sti.nasa.gov*

- E-mail your question to help@sti.nasa.gov

- Fax your question to the NASA STI Information Desk at 443-757-5803

- Phone the NASA STI Information Desk at 443-757-5802

- Write to:
  STI Information Desk
  NASA Center for AeroSpace Information
  7115 Standard Drive
  Hanover, MD 21076-1320

NASA/TM-2014-218265

Multiscale Analysis of Structurally-Graded Microstructures Using Molecular Dynamics, Discrete Dislocation Dynamics and Continuum Crystal Plasticity

Erik Saether, Jacob D. Hochhalter, and Edward H. Glaessgen
Langley Research Center, Hampton, Virginia

Yuri Mishin
George Mason University, Fairfax, Virginia

National Aeronautics and
Space Administration

Langley Research Center
Hampton, Virginia 23681-2199

May 2014

Available from:

NASA Center for AeroSpace Information
7115 Standard Drive
Hanover, MD 21076-1320
443-757-5802

Abstract

A multiscale modeling methodology is developed for structurally-graded material microstructures. Molecular dynamic (MD) simulations are performed at the nanoscale to determine fundamental failure mechanisms and quantify material constitutive parameters. These parameters are used to calibrate material processes at the mesoscale using discrete dislocation dynamics (DD). Different grain boundary interactions with dislocations are analyzed using DD to predict grain-size dependent stress-strain behavior. These relationships are mapped into crystal plasticity (CP) parameters to develop a computationally efficient finite element-based DD/CP model for continuum-level simulations and complete the multiscale analysis by predicting the behavior of macroscopic physical specimens. The present analysis is focused on simulating the behavior of a graded microstructure in which grain sizes are on the order of nanometers in the exterior region and transition to larger, multi-micron size in the interior domain. This microstructural configuration has been shown to offer improved mechanical properties over homogeneous coarse-grained materials by increasing yield stress while maintaining ductility. Various mesoscopic polycrystal models of structurally-graded microstructures are generated, analyzed and used as a benchmark for comparison between multiscale DD/CP model and DD predictions. A final series of simulations utilize the DD/CP analysis method exclusively to study macroscopic models that cannot be analyzed by MD or DD methods alone due to the model size.

Keywords: Multiscale analysis, molecular dynamics, dislocation dynamics, crystal plasticity, graded material microstructure

1.0 Introduction

Structurally-graded nanocrystalline (SGNC) materials are a new class of metallic materials that offer the promise of obtaining previously unachievable combinations of strength, ductility and toughness. The structurally-graded architecture is believed to combine the extremely high strength potential offered by traditional nanocrystalline materials with deformation mechanisms that lead to higher ductility and greater toughness as exhibited by coarse-grained (CG) materials. SGNC materials consist of layers in which the grain size varies from relatively fine (10 nm - 100 nm) to relatively coarse (100 nm – 10 μm). Here, the fine grains contribute to improve overall material strength while the coarser grains contribute to the ductility and toughness.

SGNC metallic materials have been developed over the past several decades with the promise of achieving higher strengths than are possible with traditional microstructures (Gleiter, 1989). Despite the advantage of increased strength, the long-studied disadvantages of nanocrystalline metals include their lack of ductility and their low fracture toughness (Whang, 2011). To address these shortcomings, a microstructural concept shown in Figure 1 was developed by Fang and co-workers (Fang, 2011) that offers the promise of combining the strength of nanocrystalline metals with the ductility and toughness of traditional metals. Shown in Figure 1, these structurally-graded

metallic materials consist of concentric layers around the central axis in a cylindrical specimen in which the grain size varies from relatively fine near the exterior to relatively coarse in the interior. Although the potential of graded nanostructures in aluminum (Al) or Al-alloys has not been explored, the Copper (Cu) results presented by Fang (Fang, 2011) suggest that the potential benefits are significant and that implementation in other face-centered cubic materials (such as Al) should be feasible. If a graded nanocrystalline structure can be designed, optimized and produced in structural materials such as Al, the impact on aerospace vehicle weight, durability and safety may be enormous.

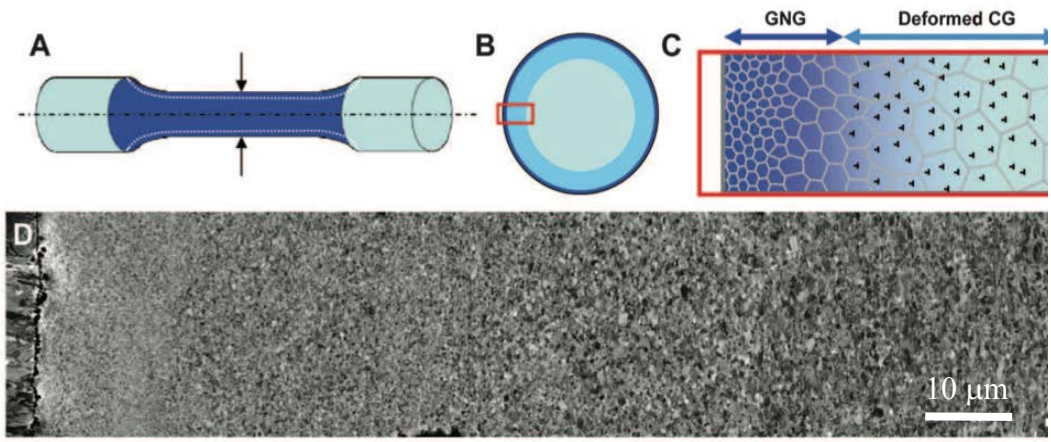

Figure 1. (A) Schematic of the tensile bar specimen. (B and C) Schematics of the cross-sectional microstructure consisting of a graded nano-grained (GNG) layer (dark blue) and a deformed coarse-grained (CG) layer (blue) on a CG core (light blue). (D) A typical cross-sectional scanning electron microscope image of a SGNC Cu sample. (From Fang, 2011)

These emerging material forms motivate the development of new computational modeling methods that can address their unique microstructural configurations and responses. Because of the small grain sizes considered, analyses developed for structurally-graded materials must be able to predict length scale effects. In addition to the well-known effects of grain size on material response in a gradient field (see, for example, Fleck, 1994), recent experimental studies (Uchic, 2009) have revealed that a grain-size dependence can also exist in the absence of gradients. Uchic (Uchic, 2009) and others have used in-situ compression studies of micropillar specimens with characteristic dimensions in the range from less than a micron to tens of microns to evaluate material flow properties and the dependence of dislocation processes on grain size.

To study the fundamental atomistic bases for deformation and failure mechanisms in graded materials, molecular dynamics (MD) provides a complete analysis of mechanisms that include damage evolution, dislocation nucleation, grain boundary strength and mobility. However, this methodology is restricted by the material domain size and time interval of interest. For example, a cubic sample of Al with side dimension of 1 μm contains over 12 billion atoms which exceeds current computational capabilities by

roughly one order of magnitude for practical simulation.

The dynamic evolution of lattice defects that are described by a multitude of dislocation mechanisms constitutes the atomistic basis for plastic deformation, toughness and strain hardening in metallic microstructures. Short-range interactions are described by local constitutive laws in which dislocations can annihilate, generate pile-ups, combine through complex junction formation, or become pinned to participate in a Frank-Read source for nucleating additional dislocations. These processes and their interactions dictate the initiation of yielding, subsequent strain hardening and development of internal structures such as shear bands, sub-cells and low-angle grain boundaries (Hull and Bacon, 2001).

Dislocations can be simulated in either a discrete or homogenized sense. Among the methods that have been developed to simulate dislocations in a discrete sense are MD and discrete dislocation plasticity (DD). MD is the obvious computational approach for domains that can represent processes of interest that involves tens to hundreds of million atoms simulated over tens of nanoseconds. MD has been used to simulate the most fundamental mechanisms of deformation and to calibrate energy and strength parameters for analyses at larger length scales (see, for example, Yamakov, 2006; Yamakov, 2009; Warner, 2007). For larger material domains with a characteristic diameter greater than approximately 100 nm, DD simulation methods have been developed to approximate the complex evolution of dislocation fields using idealized representations of the interactions between individual dislocations (Van der Giessen, 1995; Needleman, 2001).

At even larger material domains with a characteristic diameter greater than approximately 10 - 100 μm, continuum continuum plasticity methods have been developed to simulate the collective response of large numbers of dislocations where a sufficient volume of material exists to permit homogenization of the underlying dislocation-based deformation processes. These methods include strain gradient plasticity (SGP) which includes a material length scale enabling an approximation of material size effects, crystal plasticity (CP) which includes an implicit representation of plastic slip systems, and strain gradient crystal plasticity (SGCP) which addresses both material size effects and plastic slip on individual slip systems (Roters, 2010; Evans, 2009; Fleck, 1997; Hutchinson, 2000; Han, 2005a; Han, 2005b).

To calibrate a CP representation, effective stress-strain responses determined by DD analysis are then integrated with continuum CP using an optimization approach (discussed in Section 4.1) that permit large material domains to be modeled. Because of the generality of the inverse approach, there are typically several sets of optimized crystal plasticity parameters that minimize the error represented by an objective function. Consequently, mechanics-based arguments are then made to select a single meaningful set of parameters that fully define the DD-informed CP constitutive model, hereafter referred to as the "DD/CP model." In the present study, various DD/CP models are developed to simulate plastic deformation in structurally-graded material configurations.

Multiscale methods employ various computational models of the salient physics at different physical dimensions and link them across length and time scales. Generally, simulations at the lowest length scale represent fundamental material processes; analyses at higher length scales simulate accumulations, homogenizations or complex secondary interactions over larger spatial domains and longer time periods. The approach developed herein consists of the aforementioned analysis frameworks that operate at different length and time scales. At atomic length scales, MD is used to study the formation of dislocations, twins, stacking faults, grain growth and rotation, and grain boundary (GB) strengths leading to ultimate failure in microstructures composed of nanometer-sized grains. At mesoscopic length scales, DD is applied to the analysis of discrete dislocation interactions involved in yield, plastic hardening, and load transfer in polycrystal assemblages of micrometer-sized grains. Various material constants such as mobility and GB strength are determined from MD simulations. Finally, for macroscopic simulations, CP is applied where parameters are calibrated to represent the yield stress and strain hardening from DD predictions. These effective parameters are then used in continuum finite element methods (FEM) incorporating CP to analyze material domains of arbitrary size. The hierarchy of the developed multiscale methodology is shown in Figure 2.

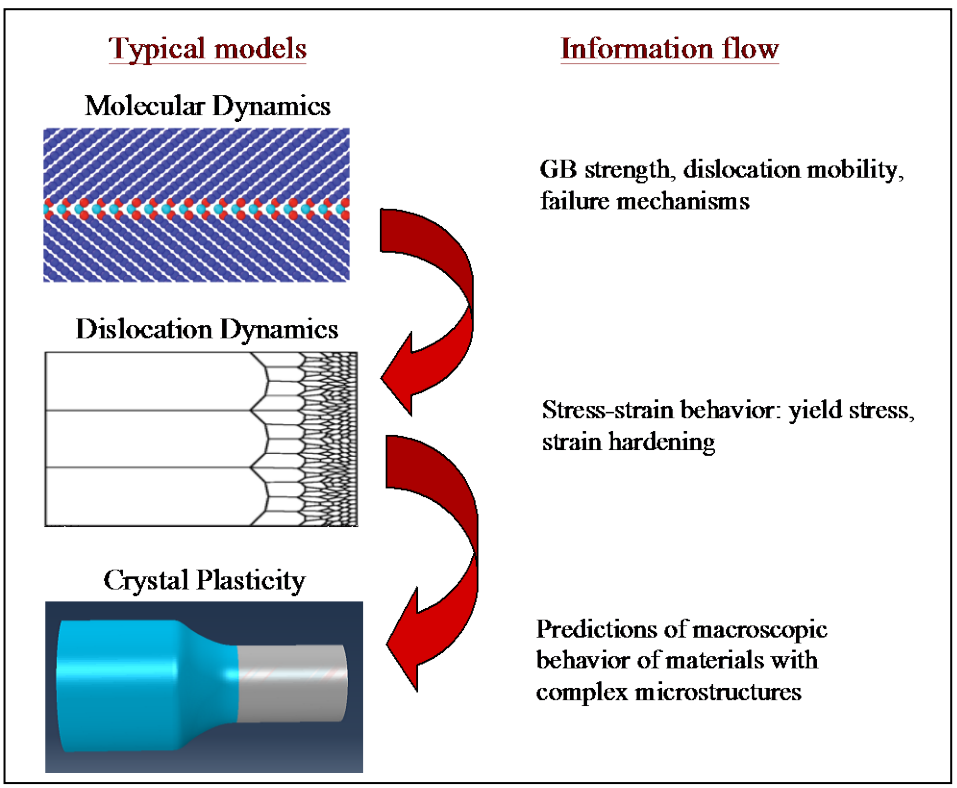

Figure 2. Hierarchy of the developed multiscale analysis methodology.

This paper is composed of the following sections. F irst, atomistic simulation of structurally-graded microstructures are performed using MD methods to determine failure mechanisms, Hall-Petch (HP) relations (Hall, 1951; Petch, 1953), and GB strengths. Second, DD plasticity and continuum CP analyses are presented. T hird, the inverse formulation is described, along with the CP parameters that were optimized to

reproduce the DD results. Fourth, results of a verification problem are discussed, where the stress-strain behavior of structurally-graded polycrystals is predicted separately using DD simulation and the DD/CP model, and then applied to macroscopic models with differing microstructural configurations that are of a size accessible to experimental validation. Finally, a brief summary of the current research is presented.

2.0 Molecular Dynamics (MD) Simulations

Al samples with uniform grain sizes ranging from 5 nm to 94 nm (containing about 40 million atoms) and having a <211> texture orientation were created by the Voroni tessellation method (Aurenhammer, 1991). The structures were equilibrated using MD simulations with atomic interactions modeled with an embedded-atom potential (Mishin, 1999). Free edge boundary conditions were applied in plane while periodic conditions were applied in the upper and lower texture directions. The simulations were performed at 300 K. A strain rate of 10^7 s^{-1} applied horizontally in the axial direction provided reasonable convergence of the results while being attainable with available computational resources. Sample uniform and graded nanocrystalline structures are shown in Figure 3.

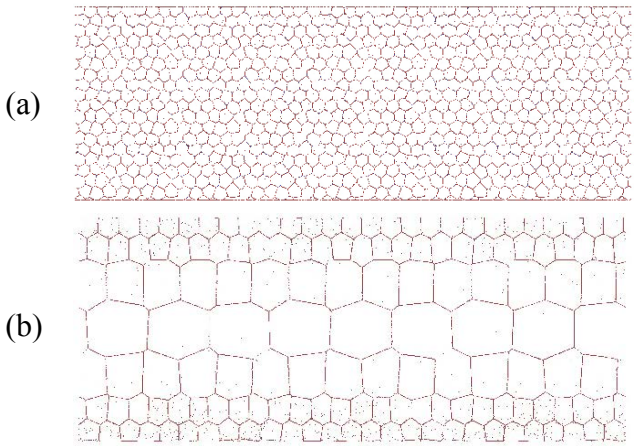

Figure 3. Examples of nanocrystalline structures in Al. (a) Uniform grain size of 19 nm. (b) Graded structure with 94 nm grain in the center and 19 nm grains near the surface.

Figure 4 shows examples of engineering stress versus engineering strain plots for uniform models with different grain sizes. Note the change in the deformation mode with the grain size, with stable flow accompanied by strain hardening at $d < 5$ nm. The occasionally observed abrupt changes in stress signify the formation of surface steps, which initiate shear band propagating across the sample. The initial peak in some of the curves reflects the "stress overshoot" effect caused by the absence of mobile dislocations in the

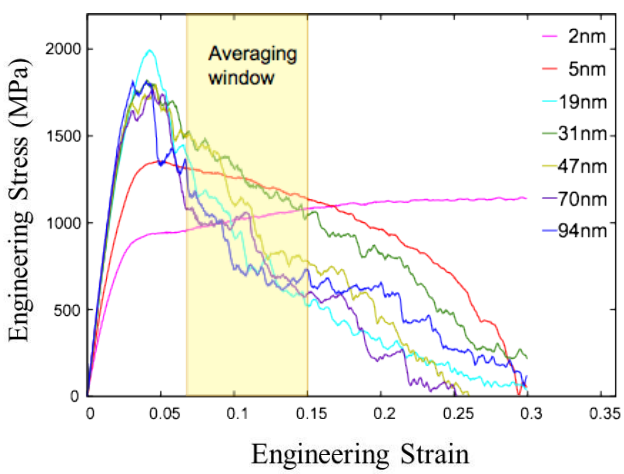

Figure 4. Examples of plots of engineering stress versus engineering strain for different grain sizes in nanocrystalline Al. The averaging window for calculation of the physical flow stress, σ_f, is indicated.

initial structures. The steady-state flow stress, σ_f, was computed by averaging the physical stress over the strain interval of 7-15%. While somewhat arbitrary, the lower value 7% avoided the stress overshoot and the upper value of 15% corresponded to the applied strain at which further strain localization caused the stress calculation to become very inaccurate. Thus, this range was used to determine the qualitative behavior of grain size vs. stress.

The grain size dependence of the flow stress is shown in Figure 5. Several models of each grain size were run to develop statistics and compute error bars. The plot reveals a maximum at the grain size of about 45 nm, which is predicted to be "the strongest size" for the <211> textured nanostructures in Al. The decrease in the flow stress, σ_f, above 45 nm is in qualitative agreement with the HP relation. This relationship was originally expressed as $\sigma_f = \sigma_0 + Kd^{-1/2}$, where σ_0 represents the strength of the single-crystal material, d is the average grain size and K is the strengthening factor. Above $d = 45$ nm, the decrease in strength with increasing grain size is due to the reduced restraint of slip by grain boundaries. Evidence of such restraint was seen in the simulations, e.g. in the form of dislocation pileups near some boundaries. The plot in Figure 5 also reveals the inverse HP effect, in which the strength decreases with further decreases in d. Examination of the nanostructures confirms that the deformation in this range of grain sizes occurs primarily by grain boundary sliding and grain rotation, with negligible dislocation activity inside the nanometer-scale grains. At larger grain sizes in the normal HP regime, the strength is largely controlled by interaction of dislocations with grain boundaries.

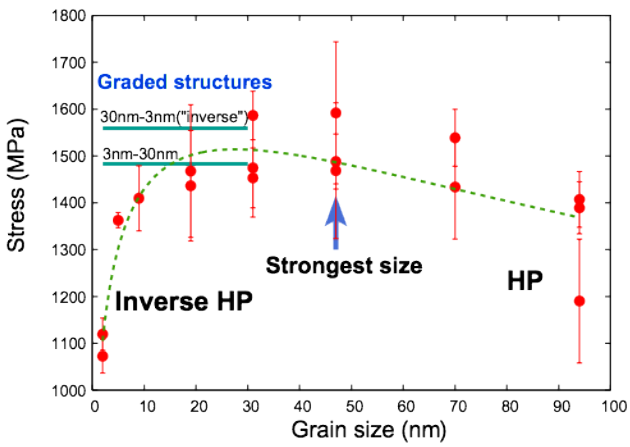

Figure 5. Flow stress of nanocrystalline Al as a function of grain size. The regions of the HP relation and inverse HP relation are indicated.

2.1 Ultimate Failure as a Function of Grain Size

It was found that, at grain sizes $d < 10$ nm under large strains ($\varepsilon > 10\%$), the samples began deforming nearly uniformly forming a wide and smooth neck that eventually reduced to a point (Figure 6a). Significant strain hardening was observed, indicating a stable flow. At larger grain sizes, the flow becomes unstable and quickly localizes in a shear band at 45 degrees to the tensile axis (Figure 6b). The material flows at a nearly constant stress in the shear band region, without appreciable strain hardening. The material fails by sliding along the shear band which becomes the fracture surface. In both modes of fracture, elongation to failure can be large (> 25%). The plastic deformation alters the grain size in the fracture zone (neck or shear band), where small grains (< 20

nm) tend to grow (strain-induced grain growth) while larger grains (> 50 nm) tend to refine by recrystallization.

Figure 7 is an example of strain localization in a shear band in a sample with d = 31 nm. Note that the grains outside the shear band are almost intact and that the severe deformation inside the shear band induces significant grain growth. A n example of graded nanostructure with grain sizes varying between 30 and 90 nm is shown in Figure 8. A snapshot of a MD simulation is shown in Figure 9 w ith various atomic-scale deformation modes identified. The accumulation of damage shows a distributed necking and strain localization. Because of the importance in discerning internal inelastic deformation, a recently developed visualization method based on tracing slip vectors (Zimmerman et al, 2001) was implemented. During MD simulation, Figure 10 shows a detailed interpretation of different important dislocation events observed using slip vectors.

(a)

(b)

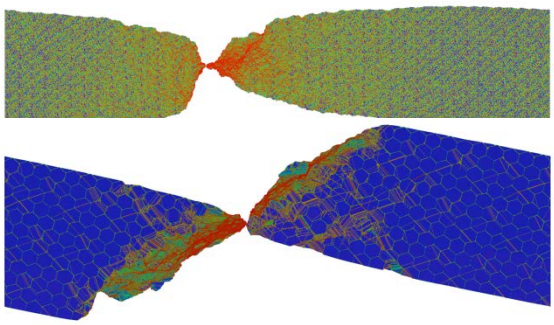

Figure 6. Illustration of two deformation and failure modes in nanocrystalline Al. (a) Grain size 2 nm, wide and smooth neck. (b) Grain size 31 nm, fracture surface formed from a slip band at 45 degrees to the tensile axis.

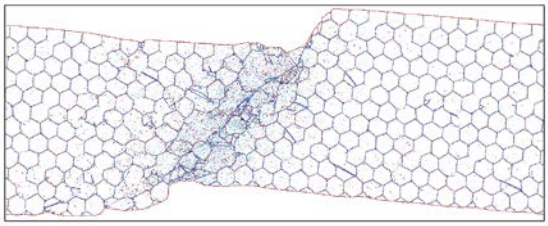

Figure 7. Example of strain localization in a nanocrystalline model with d = 31 nm.

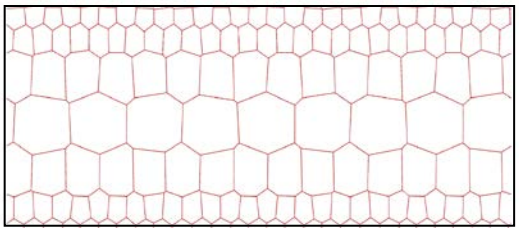

Figure 8. Example of SGNC Aluminum. The grain size ranges from d = 30 nm to 90 nm.

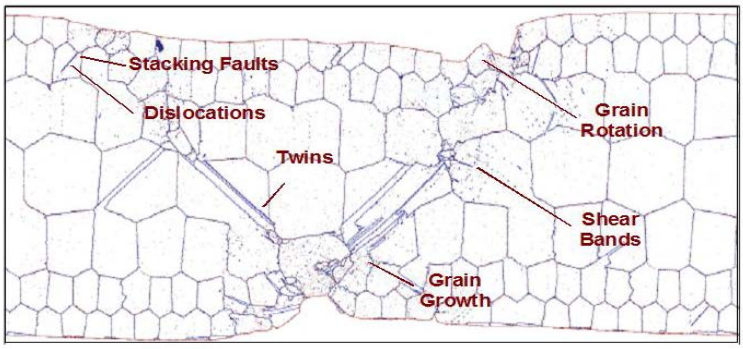

Figure 9. Strain localization in SGNC Aluminum showing fundamental deformation processes.

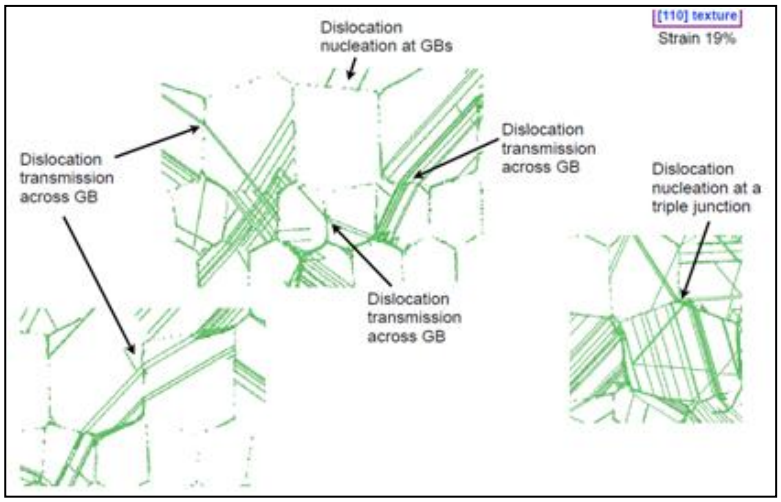

Figure 10. Interpreting important dislocation events using a slip vector visualization approach.

2.1.1 Apparent Failure Progression in Graded Microstructures

Considering a cylindrical rod specimen with a graded microstructure, an actual SGNC material would have a distribution of grain sizes that varies along a radial line from the center. However, to simplify the discussion, the microstructure is simplified into a discrete outer layer that is composed entirely of small grains and an inner layer that is exclusively composed of large grains. This idealized cross section of a graded material microstructure is depicted in Figure 11.

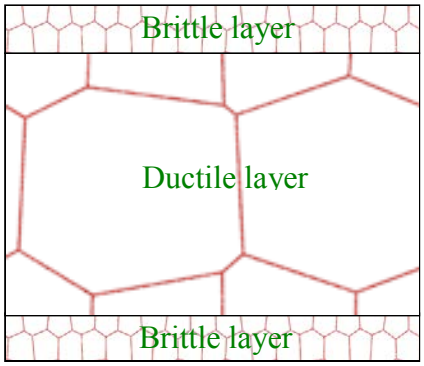

Figure 11. Simplified depiction of a graded material microstructure.

The discussion of apparent failure progression assumes direct HP behavior such that grains are above 45 nm as shown in Figure 5. For smaller grains in the inverse HP regime, failure mechanisms are primarily associated with GB sliding, migration and grain rotation. Thus, with a reduction in grain size below ~45 nm, materials tend to exhibit increased ductile response to applied loads with lower flow stresses. For grains in the direct HP regime, the material's response is dominated by mechanisms in the grain bulk that are primarily associated with dislocation nucleation and interaction. In this regime, which is currently representative of typical metallic microstructures, smaller grains are less accommodating of stable dislocation loops at lower stresses and, thus, exhibit a brittle response up to the initiation of GB migration mechanisms. Larger grains permit dislocation loops to be created at lower applied loads and allow greater magnitudes of dislocation glide in the grain interior to exhibit greater ductility due to bulk dislocation-based processes. Dislocation production in uniform grain models is depicted in Figure 12.

In the small grain model shown Figure 12a, several dislocations have been identified within dashed circles indicating a low degree of dislocation production. In contrast, Figure 12b shows a larger grain model in which dislocation nucleation is widespread.

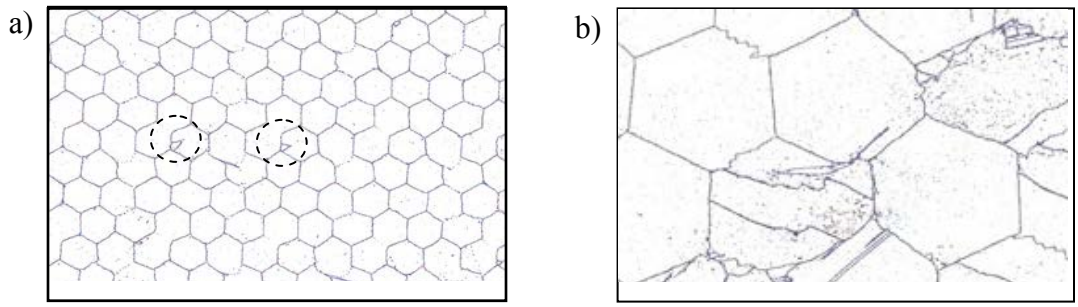

Figure 12. Dislocation production in small grain (a) and large grain (b) microstructures.

The outer layer is composed of nanoscale grains (10 nm-100 nm). Regarding deformation due to dislocations, small grains do not generate high dislocation densities. Nucleation sources in the grain – such as Frank-Read mechanisms - would require a high applied external stress to generate a stable loop, and GB sources, whether active only at junctions or associated with steps distributed along a grain surface, would be expected to generally require a high nucleation stress as a function of the angle mismatch between adjacent grains. Whatever dislocations are nucleated, the small grain diameter is the maximum distance to accumulate slip deformation before dislocations reach and participate in some reaction mechanism with a GB. However, aside from dislocation slip within a grain at higher strain levels, several other mechanisms operate to generate ductility in uniform nanocystalline materials. These include GB sliding, diffusion and stress-based GB migration, and grain rotation.

In a graded material, the small grained layers are supported by underlying layers of larger grains and deform coherently without generating any surface cracks (Fang, 2011).

The inner layer is composed of relatively large grains (100 nm - 2 μm) that exhibit ductile behavior with significant strain energy absorbed through internal deformation due to slip. The nucleation of dislocations is principally due to the Frank-Read mechanism which, due to the larger grain volume, can operate at low applied stress levels and produce a large number of dislocation loops that have the dimensional freedom to glide significantly before encountering a GB. The effect of microstructural mechanisms on overall stress vs. strain response is significant. Figure 13 shows a qualitative comparison of the stress-strain response of materials composed of different microstructures.

Material failure, in general, originates from a distribution of defects or weak links at lower length scales that coalesce to form damage regions at the highest length scales that precipitate catastrophic failure. At each length scale, material damage causes strain localization that intensifies local stresses and provides additional energy to propagate existing damage processes. Damage progression can be unstable or stable; in unstable propagation, subsequent failure after initial damage occurs at the same or lower stress

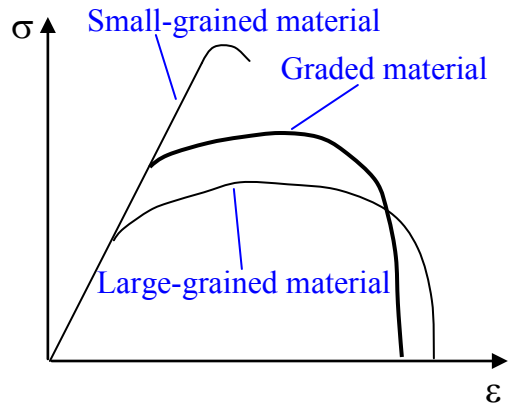

Figure 13. Schematic stress-strain relations for materials with different microstructures.

level and quickly leads to ultimate failure; for stable propagation, the energy required to continue failure progression is greater than that required to initiate damage. For example, a complex structure can possess multiple load paths in which a local failure can redistribute internal loads such that additional failure is avoided; this constitutes the desirable feature of damage tolerance.

In a graded microstructure, the different sized grains form effective barriers to damage propagation. Three stages may be loosely identified along the stress-strain curve as depicted in Figure 14. These stages are characterized by the interaction of different failure mechanisms operating spatially in the microstructure.

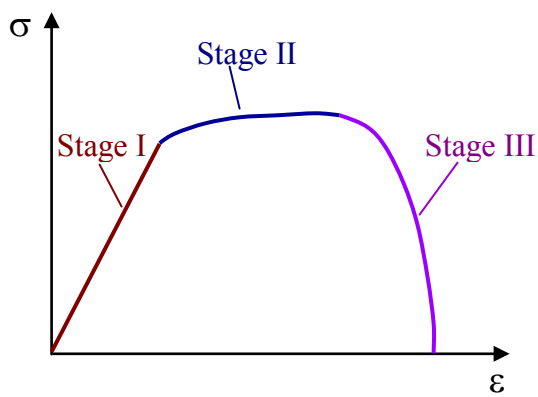

Figure 14. Stages identified in the stress-strain relation of a graded material corresponding to primary failure mechanisms operating in the microstructure.

During Stage I, the material exhibits a linear elastic response prior to yield. Figure 15 depicts a microstructure during this initial stage in which no internal damage is generated due to mechanisms such as dislocation nucleation.

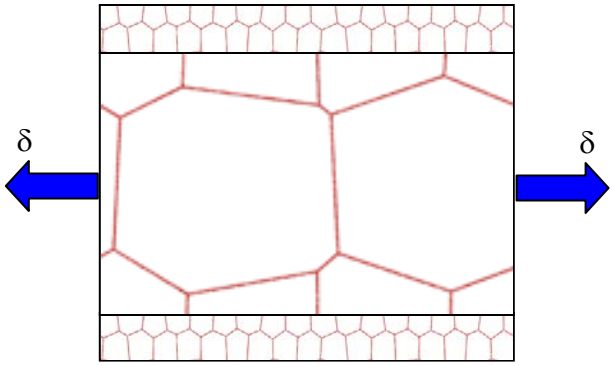

Figure 15. Linear-elastic behavior prior to yield in Stage I.

In Stage II, yield begins in the inner layers due to dislocation nucleation but is constrained by the layers with nanocrystalline grains. Large grains generate dislocation slip at low stresses that propagate and pile up along GBs. Step formation in the GBs can transmit slip directly or dislocations can pile-up along GBs that can increase stresses in the adjacent grain such that new dislocations are nucleated. However, if the adjacent grains are small, dislocation nucleation energy can be high and the layer of small grains effectively reduces the propagation of slip deformation. This impedance to damage propagation is a barrier that sequesters deformation processes within the inner layer until a higher load is reached at which other deformation mechanisms in the nanocrystalline layers are initiated. The constraining of inner layer slip is depicted in Figure 16. Thus, strain localization and stress intensification are blocked to some degree from propagating away from the inner ductile layer and stabilize the global material deformation. Assuming displacement-controlled loading, the stress-strain response exhibits yielding with subsequent strain hardening that result from load being transferred to the stronger outer layers. Without the stiffer outer NG layer, plastic yielding would quickly produce necking across the entire cross section leading to ultimate failure.

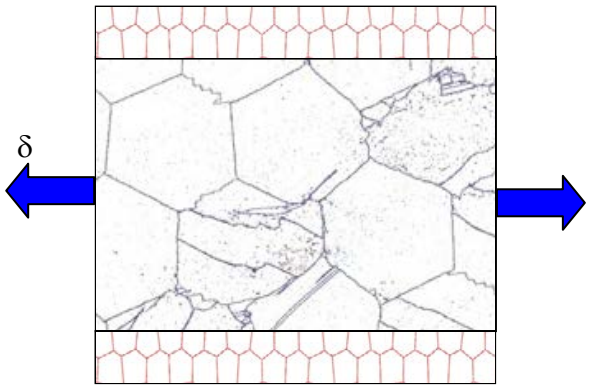

Figure 16. Constrained inner layer slip failure corresponding to Stage II.

In Stage III, stresses in the outer nanocrystalline layers become large enough to cause GB sliding, migration, and grain rotation. This typically begins at a particular site in the outer layer at a ‘weak link‘ and allows strain localization due to deformations in the inner layer

to extend to the surface causing a l ocal increase in axial strain. This elongation necessarily decreases the area of the cross section due to volume conservation and moves the small grains inward towards the center, beginning an overall necking of the specimen. While deformation mechanisms still vary from predominantly dislocation production and interaction in the interior to GB slip, migration and rotation at the exterior, it is assumed that the stresses tend to become more uniform over the cross section and the stabilizing effects of a graded microstructure is essentially lost. The specimen then approximately behaves as a homogeneous material in which necking progresses until final catastrophic failure. In this stage, the bi-layer simplification used for earlier deformation stages is no longer used and the failure processes occurring through all graded layers are depicted as shown in Figure 17.

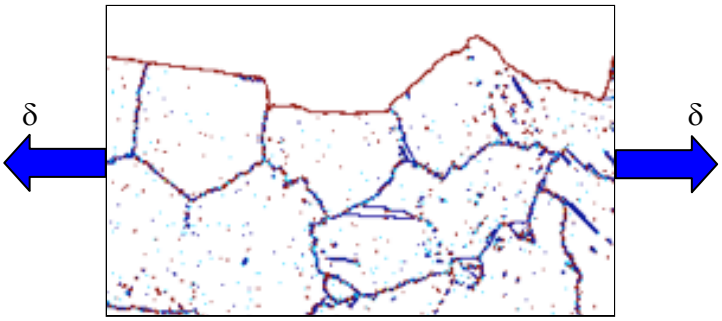

Figure 17. GB slip, migration and grain rotation in the outer nanocrystalline region corresponding to the onset of Stage III.

The combined state of various damage mechanisms lead to an overall necking of the specimen as depicted in Figure 18. These mechanisms operate across the specimen thickness during Stage III and generate a more uniform stress state before the precipitation of final failure.

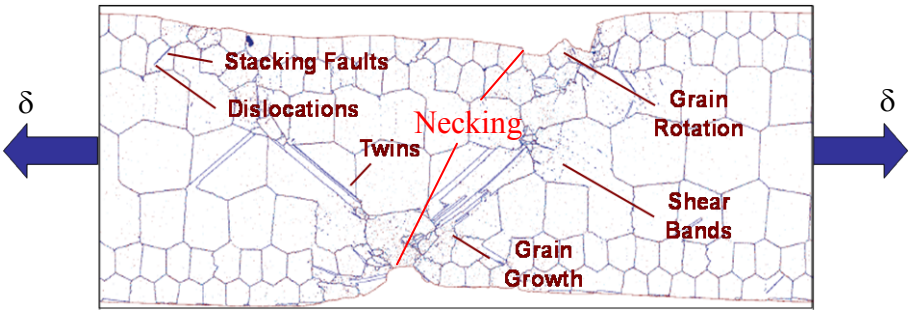

Figure 18. Combined deformation mechanisms active in causing final failure.

In general, the improved behavior of the graded material microstructure under axial loading examined here appears to be attributable to a mixture of different responses of the large and small grain layers that is similar to the behavior of laminated composite materials in which overall constitutive properties or the failure sequence can be guided through the choice of ply layer stacking sequence. Through Stage II, the small surface grains provide a higher stiffness before exhibiting an initiation of failure which increases the overall yield strength of the material. The interior large grains respond with a large

ductility (toughness) that is constrained against propagation through the cross section by the stiffer outer layer. At the onset of Stage III, all damage mechanisms are free to operate and strain localization spreads through the material thickness by different deformation mechanisms prior to ultimate failure. Thus, a graded material can exhibit a higher yield stress and toughness than a freestanding specimen composed entirely of large or small grains.

2.2 Dislocation Transmission

To simulate the interaction of dislocations with GBs, a six layer MD model was developed. The interface between each layer constituted a s ymmetric tilt boundary. Figure 19 depicts a Σ5 boundary that is used to quantify dislocation transmission. The model has periodic boundaries on the upper and lower surfaces with free edge boundaries on the right and left sides. The triple junctions at the free edges served as dislocation sources. There is only one (111) slip plane of ½[110] dislocation in each grain and this model was used to investigate dislocation interactions with individual GBs. A schematic of this model showing four representative layers containing Σ5 grain boundaries is depicted in Figure 20.

Under an applied tensile stress, dislocations nucleate from triple lines at the surface and interact with the grain boundaries. Most of the attempts are unsuccessful - the dislocation returns to the source. Some dislocations transmit through a GB but then return to the surface. Eventually, at small stresses, the grain boundaries stop further propagation of the dislocations. At a critical value of the stress, dislocation transmission through grain boundaries begins as illustrated in Figure 21. After each transmission event, the dislocation leaves a damaged region in the boundary, which concentrates the stress and promotes further nucleation from the same boundary region. This generates a new GB source that can nucleate additional dislocations and is depicted schematically in Figure 22. The rapid multiplication of dislocations leads to the formation of slip bands from which a dominant band develops and forms a fracture surface across the cross section.

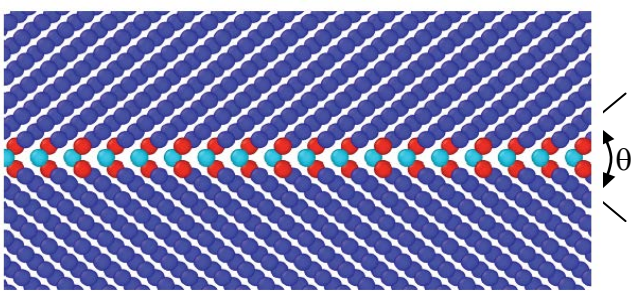

Figure 19. Σ5 grain boundary configuration, the tilt angle is θ = 78.46°.

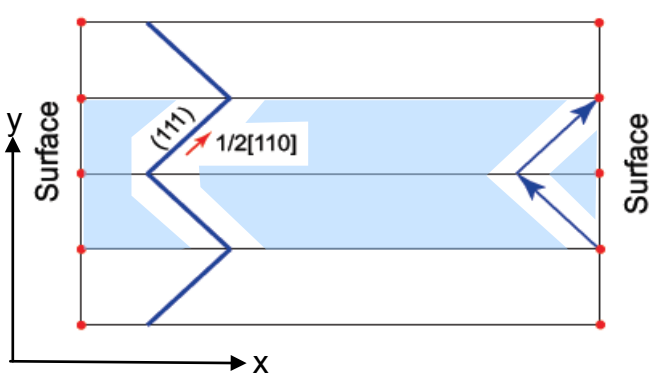

Figure 20. Model used for MD simulation of GB strength.

Figure 23 shows a trace of a dislocation generated from a surface junction and subsequently absorbed by a GB. After absorption into the GB, the distortion to the interface atoms spreads and can become a nucleation site for dislocation transmission with a shift as depicted in Figure 24.

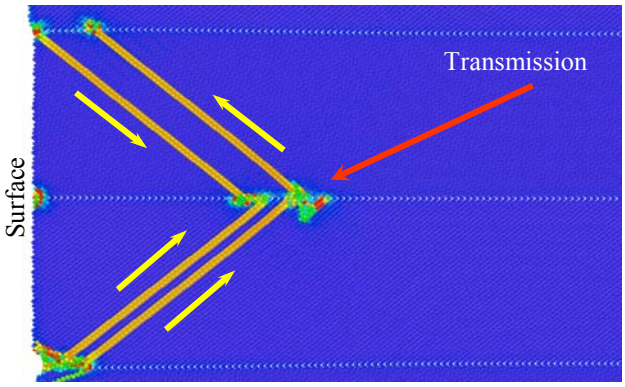

Figure 21. Example of dislocation transfer across a Σ5 grain boundary in multi-layered nanocrystalline Al.

The model shown in Figure 20 is initially defect free in the bulk fcc crystal. In addition, the GB structure is idealized with no irregularities - such as jogs or forest dislocation fragments - other than the distortion at the grain interface described by the Σ angle. The strength of the GB is therefore high, indeed the change in density along a GB might vary by less than 5% for an arbitrary GB configuration, thus preserving most of the metallic bonds with small deviations from equilibrium spacing in a perfect lattice.

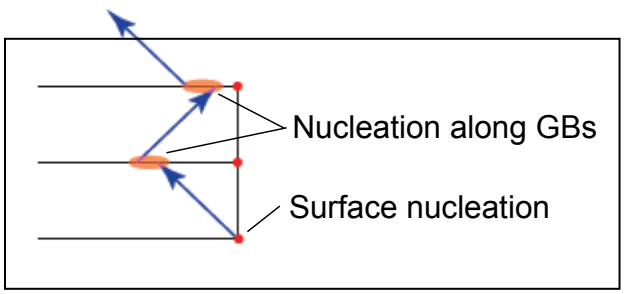

Figure 22. Mechanisms for dislocation nucleation.

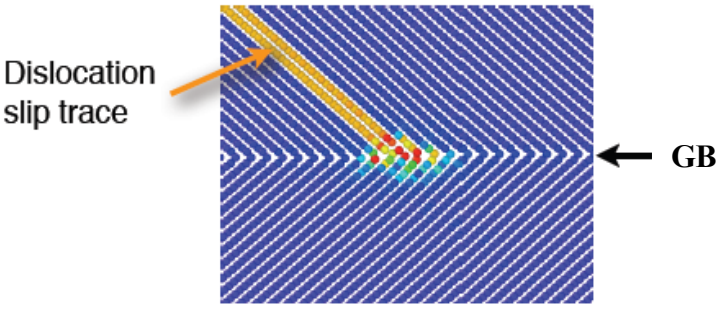

Figure 23. Dislocation absorption at a GB.

Stress-strain curves for the Σ5 GB is shown in Figure 25 at two different applied strain rates. The curve shows the relationship between the normal stress, σ_{yy}, and normal strain, ε_{yy}. It is observed that no significant strain rate effects were found and that the strength of the model used is high, approximately 2.8 GPa, after which dislocation nucleation lowers

the internal stress associated with the applied strain. This model thereby effectively predicts the strength properties of the Al material domain exclusively based on dislocation interaction with the GB which may then be assigned to models appropriate for simulation at larger length scales. For a Σ5 GB, the angle offset is 78.46^{o} that yields a Schmid factor of 0.196. Dislocation mobility is a function of the resolved shear stress along a slip plane and yields a peak shear stress of 0.56 GPa which is subsequently used in DD simulations.

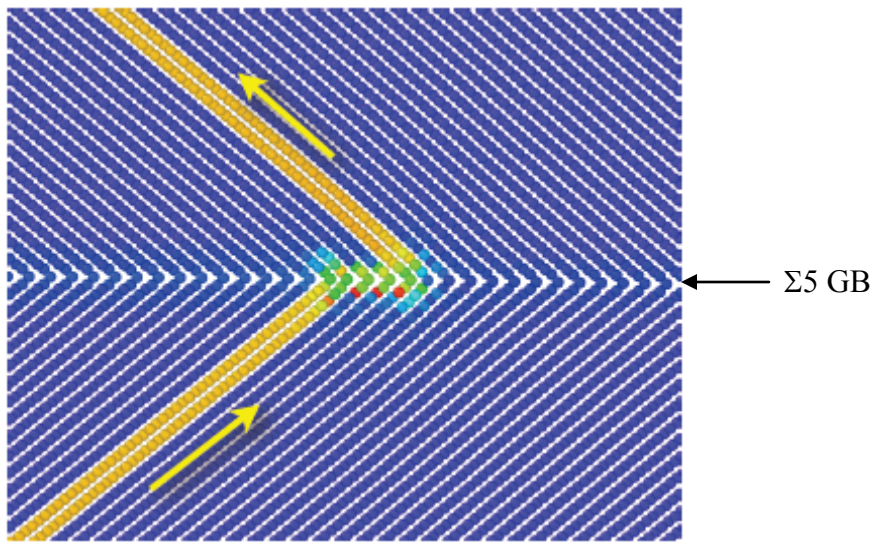

Figure 24. Dislocation transmission with a shift.

A detailed analysis of the MD simulation of stress-strain behavior during the early stages of deformation is shown in Figure 26. The results shown were obtained at a strain rate of 10^6 s^{-1} and show the comparison of normal stress with dislocation state in the material domain. Snapshots of dislocation activity at various stress levels are also shown.

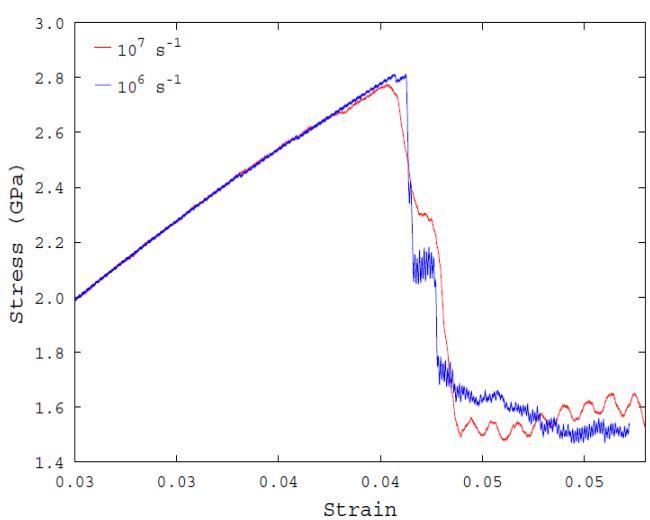

Figure 25. Stress-strain curves for Σ5 GBs in Al.

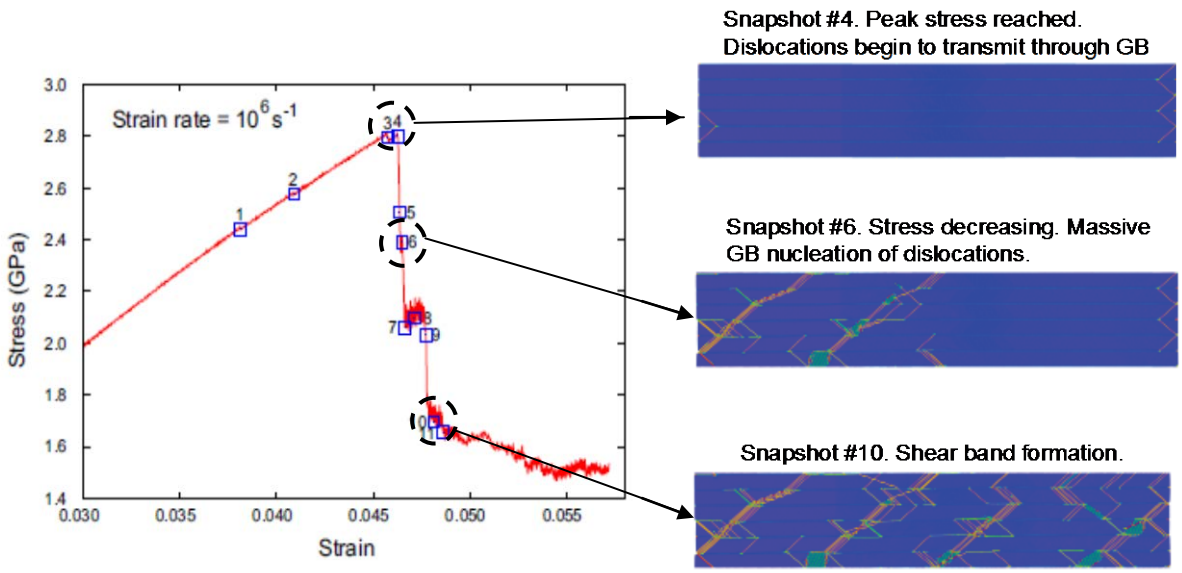

Figure 26. MD simulation of deformation states and stress-strain prediction.

3.0 Dislocation Dynamics (DD) Analyses

Discrete DD simulations may be performed in either two or three dimensions. In two-dimensional simulations, dislocation loops are represented as dipole pairs that are constrained to glide along a specified subset of available slip planes. The result is a simplified representation that simulates dislocation interaction and the resulting plastic hardening behavior of the material. Benzerga (Benzerga, 2004) has developed representations of three-dimensional mechanisms such as junction formation, dynamic sources and shearable obstacles in the form of two-dimensional analogues. These mechanisms have been incorporated into the present analysis. While the inelastic stress-strain and hardening behavior is a main outcome of the analysis, much investigation has also been performed to determine the formation of dislocation structures such as sub-cells, shear bands and low-angle grain boundaries (Devincre, 2001; Mughrabi, 1983; Thomson, 2002). These internal structures are generated by the plastic deformation of the material and, if they participate as additional constraints on dislocation mobility, increase the hardening and toughness of the material.

The dependence of yield stress on grain dimension is quantified by the HP relation whereby ductility tends to increase and yield stress tends to decrease with increasing grain size but this trend is reversed when grain size falls below a minimum size in the "inverse" HP regime (Freidman, 1998; Zhu, 2006). Other grain size-dependent deformation mechanisms (Evers, 2002; Gavriljuk, 1999; Li, 1970) have been observed and are implicitly considered in the present DD simulation including:

- Dislocation pile-up: Decreasing grain size causes the number of dislocations piling-up against a grain boundary to be reduced. As a result, the stress concentration at the grain boundary is lowered which lessens nucleation of new dislocations in the neighboring grain.

- Reduction in slip magnitude: Decreasing grain size reduces the mean free path for dislocations and results in higher strength with reduced ductility.

- Constrained nucleation: Decreasing grain size causes a reduction in the overall production of dislocations, most of which nucleate along grain boundaries. This contrasts with the high availability of Frank-Read sources in larger grains that permit less constrained dislocation generation and associated plastic flow.

- Source extinction: This effect is common in nanocrystalline materials and is caused by a geometric constraint wherein small grains can only accommodate small dislocation loop diameters. As a result, high local shear stresses are required to nucleate dislocations at a separation distance that is sufficient to avoid collapse of the dipole pair and cause immediate annihilation.

In the analysis of the two-dimensional domain shown in Figure 27, the material is assumed to be pure Al loaded uniaxially to 0.5% tensile strain in the *y*-direction and three slip planes were selected with orientations of 60, 0, -60 degrees. The choice of orientations is only constrained by rotation around an axis normal to a {111} plane in the fcc metal which defines a cut plane positioned to intersect three of the 12 available slip planes at an equal angle. This configuration is similar to the hexagonal crystal used by Miller (Miller, 2004). Elastic properties and the other parameters used in the DD simulation are listed in Table 1.

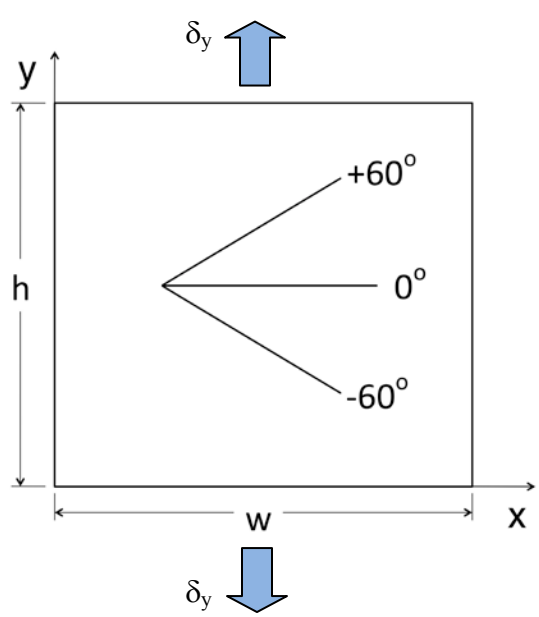

Figure 27. Model domain showing slip plane orientations.

Table 1.
Numerical constants, material properties, and load parameters for aluminum.

Parameter	Symbol	Value
Time step	Δt	0.25 ns
Shear modulus	μ	25.3 GPa
Poisson's ratio	ν	0.341
Burgers vector	b	0.285 nm
Source strength	τ_s	0.027 GPa
Obstacle strength	τ_o	0.08 GPa
Standard deviation	sd	0.2
Nucleation time	t_{nuc}	10.0 ns
Core diameter	c	6b nm
Capture distance	l_{cd}	6b nm
Slip plane separation	l_{slp}	100b
Velocity cut-off	v_{max}	100 m/s
Mobility factor	B	1.0×10^{-4} Pa s
Dynamic source probability	p_{ap}	0.04

An effective stress, $\overline{\sigma}_{yy}$, is determined by integrating the dislocation stress fields over the segment of the boundary at which an effective strain, $\overline{\varepsilon}_{yy}$, is applied. The resulting stress-strain response is computed using

$$\begin{aligned} \overline{\varepsilon}_{yy} &= \delta_y / h \\ \overline{\sigma}_{yy} &= \frac{1}{w} \int_0^w \sigma_{yy}(x)\, dx \Big|_{y=h} \end{aligned} \tag{1}$$

For a polycrystal model, the effective stress is obtained by applying Equation (1) for each grain along the outer boundary and averaging along the length of the model. The computation of an effective stress becomes

$$\overline{\sigma}_{yy} = \frac{1}{L}\left[\sum_i^N l_i \int_{L_{I-1}}^{L_i} \sigma_{yy} dx\right] = \frac{1}{L}\left[\sum_i^N l_i \overline{\sigma}_{yy,i}\right] \tag{2}$$

where N is the number of boundary grains, L is the total length given by the sum of individual grain lengths, l_i, along the outer boundary as

$$L = \sum_i^N l_i \tag{3}$$

3.1 Representation of GB-Dislocation Interactions

The range of different atomic structures comprising GBs in metallic materials is large and significantly affects the energetics and characteristics of dislocation-GB interactions. The interactions occur through a variety of mechanisms that must be considered in the DD simulations. Dislocation-GB interactions can be represented by a combination of reflection, absorption and transmittance (Shen, 1988) in DD analyses as depicted in Figure 28.

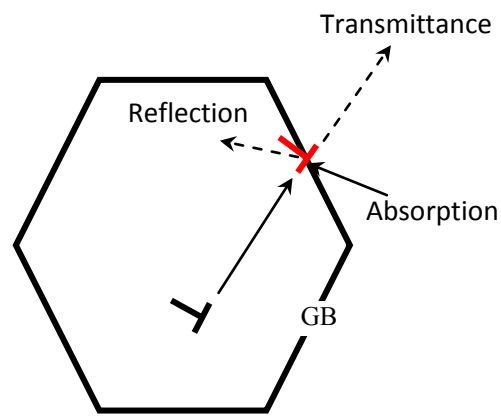

Figure 28. Dislocation-GB interactions.

In DD analysis, reflection can be simulated by preventing dislocations from crossing a GB and allowing them to freely glide away along their incident slip plane angle. Absorption can be simulated by pinning dislocations at the GB. Transmittance can be simulated by allowing dislocations to enter an adjacent grain when crossing an internal GB in a polycrystal model. Dislocation-GB interaction can be complex as suggested by the schematic in Figure 29 for a Σ3 GB presented by Abuzaid (Abuzaid, 2012). For partially transmitted dislocations, the residual Burgers vector retained at a GB plane is directly related to GB resistance against slip transmission, thereby increasing plastic strain accumulation and hardening response. Dislocations that have exited the external boundary of the material domain are held at the boundary, although their stress fields are set to zero. For dislocations transmitted across a GB into a neighboring grain, the placement within the new slip system is made such that the change in angle between the original and new slip plane is a minimum (Clark, 1992). In the present work, the effect of both reflective and transmissible GB properties were explored.

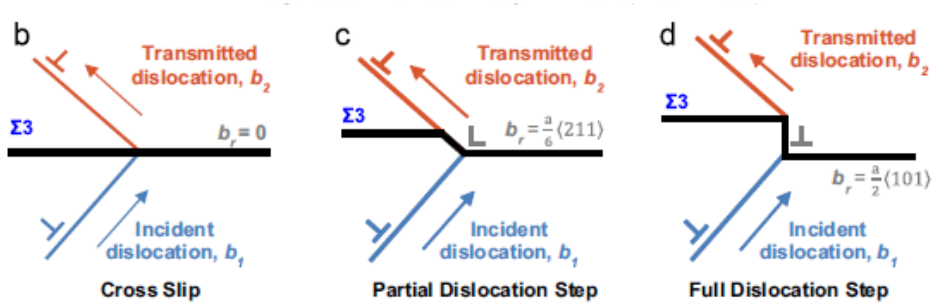

Figure 29. Schematic of the range of GB-dislocation interaction mechanisms. (From Abuzaid, 2012)

The elastic properties of GBs have been shown to have significant spatial variation on the atomistic scale (Adams, 1989; Schiotz, 1999; Wolf, 1993). However, the thickness, $t_{GB,}$ of a GB is very small (on the order of 1 nm) and, in a polycrystal configuration, relative normal and tangential movement of adjacent grain surfaces is negligible prior to Stage III deformations that are dominated by GB migration. Thus, for small applied strains, both normal and shear stress components are assumed to be fully transmitted across GBs and the integration of long-range stress fields to determine the contribution of forces on dislocations in one grain from those in surrounding grains is not invalidated by any discontinuities caused by the presence of an interposed GB.

4.0 Continuum Crystal Plasticity Formulation

Because the MD simulations were performed near the upper limit of system sizes that can be considered by current massively-parallel atomistic simulations (NASA/Pleiades, 2013), DD was employed for the study of larger material systems with results of simulations mapped into parameters that form the basis of a CP representation.

An elastic-viscoplastic CP formulation that followed the work of Matouš and Maniatty (Matouš, 2004) was implemented within a continuum finite element analysis. A brief overview of the CP constitutive model is given here, but is strictly limited to aspects that are necessary for subsequent discussion. A recent review of crystal plasticity models can be found in Roters (Roters, 2010).

The CP constitutive model used here is composed of a multiplicative decomposition of the total deformation gradient, F, into its elastic, F^e, and plastic parts, F^p. A power-law slip rate equation is used to determine the evolution of slip, $\dot{\gamma}^{\alpha}$, on the systems, α, given by

$$\dot{\gamma}^{\alpha} = \dot{\gamma}_o \frac{\tau^{\alpha}}{g^{\alpha}} \left| \frac{\tau^{\alpha}}{g^{\alpha}} \right|^{\frac{1}{m}-1} \tag{4}$$

Hardness is represented by the Voce-Kocks hardening model and is computed as

$$\dot{g} = G_o \left(\frac{g_s - g}{g_s - g_o} \right) \dot{\gamma} \tag{5}$$

All parameters used in Equations (4) and (5) are identified in Table 2. The Voce-Kocks hardening model enforces all slip systems to begin with the same hardness and subsequently harden at the same rate; consequently, the α superscripts have been dropped in Equation (4). This hardening model has been used in previous crystal plasticity studies of Al polycrystal deformation (Matouš, 2004).

Table 2. Crystal Plasticity Parameter Definitions.

α	The slip system
$\dot{\gamma}^{\alpha}$	The time rate of slip
$\dot{\gamma}_0$	The reference slip rate
τ^{α}	The resolved shear stress on system α
g^{α}	The current hardness on system α
m	The rate sensitivity parameter
G_o	The hardening rate parameter
g_o	The initial hardness
g_s	The saturation value of the hardness

4.1 Mapping of DD Simulation Results to CP Parameters

In the present multiscale modeling approach, CP parameters are calibrated to the stress-strain behavior of a series of DD simulations using different grain sizes. The parameterized CP model using DD results is denoted 'DD/CP.' In mapping the higher fidelity results obtained from DD simulations to the lower fidelity continuum CP parameters, the governing equations available in the CP formulation yield an optimization problem in which the CP parameters are selected to minimize the difference between the stress-strain predictions made by the DD/CP and DD models.

The Design Optimization Tools (DOT) library (DOT, 2011) was used to link a gradient-based optimization to a finite element simulation code. The finite element model was subjected to the same uniaxial loading as the DD model and was analyzed with free edge boundary conditions along $x = 0$ and $x = w$ in Figure 27. In the optimization procedure, the DD-simulated stress-strain behavior was used as the target solution and the CP parameters were varied until a minimum difference between the CP- and DD-predicted stress-strain curves was reached within a set tolerance. This process was repeated for each grain size.

The CP model of Matouš (Matouš, 2004) contains 15 material parameters that must be considered during the optimization. Three of the parameters are the Euler angles defining the grain orientation with respect to specimen coordinates and another three parameters are anisotropic elasticity constants. None of these six parameters are included in the optimization because they can be determined directly. Thus, nine parameters remain to capture various aspects of plastic behavior. Two primary characteristics of plastic hardening behavior were observed to vary in the DD-predicted stress-strain behavior. The first characteristic is the initial hardening rate just after dislocation nucleation and is included in the analysis by calibration of the parameter g_o in Equation (5). The second characteristic is the overall strain-hardening rate and is included in the analysis by calibration of the parameter G_o in Equation (5). The remaining CP parameters were kept

constant for all DD models since they were assumed to be independent of the grain size. Those values that were not optimized were set equal to values used in Matouš (Matouš, 2004) for pure Al. The optimized parameters, G_o and g_o, are plotted as a logarithmic function of grain size in Figure 30. T he logarithmic equations fitted to the calibrated parameters can be used as input to the DD/CP polycrystal simulation, effectively incorporating the DD-predicted size-dependent stress-strain behavior. The resulting functional form is used to develop the DD/CP formulation and implicitly account for both the various mechanisms involved in the evolution of dislocations and the dynamic interactions of those dislocations. The optimization is depicted schematically in Figure 31 and a sample fit between CP and DD stress-strain predictions is shown in Figure 32.

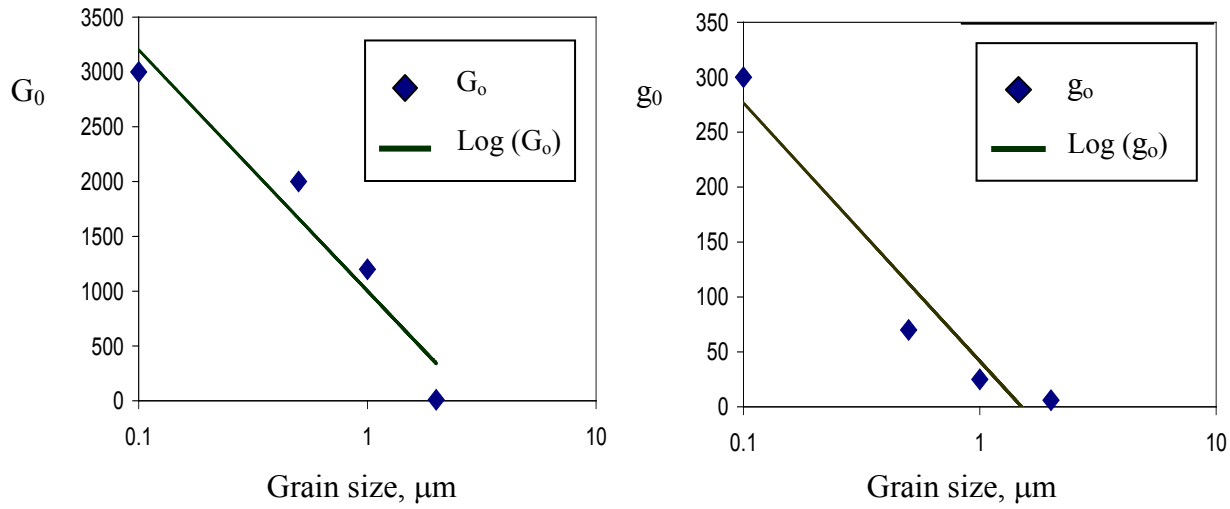

Figure 30. The calibrated functions G_o and g_o determine the evolution of hardness in DD/CP simulations.

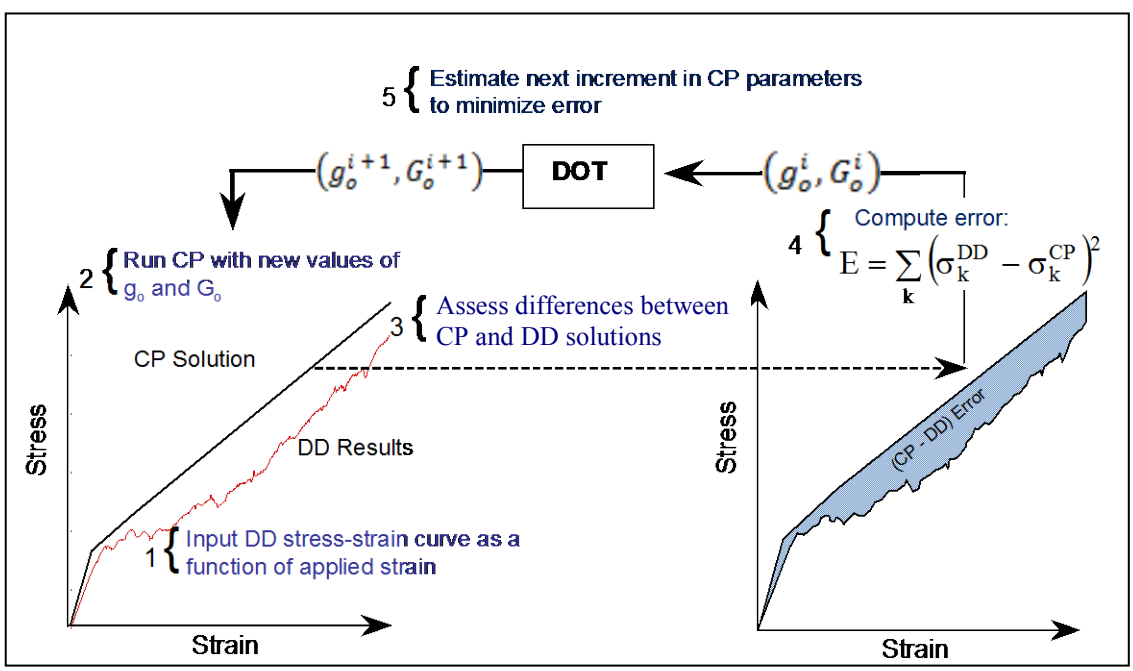

Figure 31. Schematic of optimizing CP parameters with DD results using DOT.

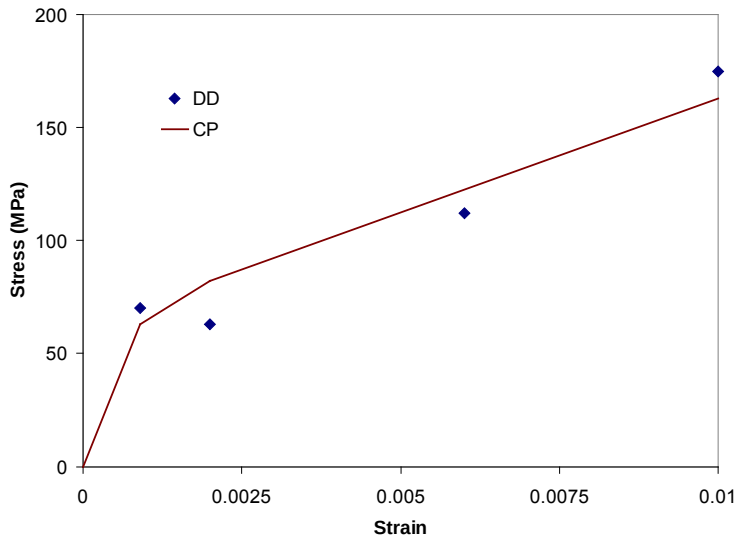

Figure 32. CP fit to DD stress-strain curve.

5.0 Polycrystal Simulations using DD Analyses

Various monocrystal and polycrystal DD simulations were performed to address different theoretical issues that are described in the following subsections. Section 5.1 details the generation of two series of monocrystal DD models that assumed solely reflective GB-dislocation interactions and employed periodic boundary conditions to simulate infinite material domains. The first set of simulations on monocrysal models was performed to obtain stress-strain relations as a function of grain size to verify that HP effects were being represented. The second set of simulations was performed using similar monocrystal models to map yield stress and strain hardening behavior into effective CP parameters. Section 5.2 discusses the generation of idealized graded DD and CP polycrystal models incorporating mapped parameters to compare the overall predictions of stress-strain response between the two simulation methods. Section 5.3 details the construction of a polycrystal DD model using Voronoi tessellation. While the tessellation produced more realistic grain geometries, the shape of the grain however does not affect DD results. The model assumed transmissible properties that would permit dislocations to glide into adjacent grains if the GB energy barrier was exceeded. This model was used to predict load transfer from the large grains in the interior to the small grains in the region along the exterior boundary. This simulation suggested that the increase in strength is due to the stiffer, brittle behavior of the small grains along the exterior and that the preservation of toughness is due to the ductile response at higher loads of the larger grains in the interior. Section 5.4 presents the generation of an additional set of square grained polycrystal models that assumed transmittable GB properties. A new mapping of the DD stress-strain behavior to effective CP parameters was made by perturbing the parameters determined in Section 5.2. Finally, Section 5.5 presents a preliminary investigation into strain rate effects in DD simulations.

5.1 DD simulations of the HP effect and mapping of CP parameters

The DD model was constructed to be free of finite edge effects in order to simulate bulk material behavior for mapping DD simulation results to continuum crystal plasticity parameters. H ence, periodic boundary conditions (PBCs) were applied in which a central DD domain is replicated as image cells in both in-plane directions. All images contribute to the stress calculation at dislocations in the central cell and the summation of stresses is carried out to a s pecified number of image layers. A schematic of the basic configuration used in applying PBCs is depicted in Figure 33.

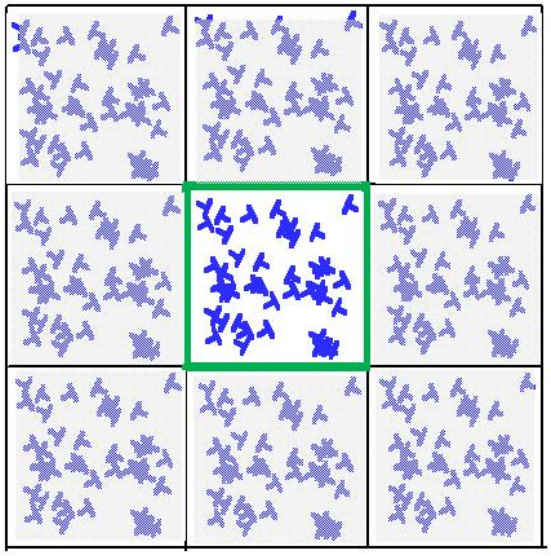

Figure 33: A central DD domain surrounded by periodic images to represent a boundary-free material.

DD simulations were performed on square grains with side dimensions d = 10.0 μm, 2.00 μm, 1.00μm, 0.71 μm, 0.45 μm and 100 n m. Three slip systems were maintained at orientation of 60, 0, -60 degrees. The DD simulations were started without pre-existing dislocations but with an initial source and obstacle density of 4.5 x $10^{13}m^{-2}$ and 1.5 x $10^{13}m^{-2}$, respectively. The selected values represent moderately low initial densities but were found numerically adequate to demonstrate different grain behavior as a function of grain size over the range of interest. Both dislocation pile-ups at the GB and pinning due to obstacles in the grain interior were simulated; however, nucleation of dislocations from GBs was not considered. Loading was applied uniaxially in tension to 1.0% strain and the resulting stress-strain curves are shown in Figure 34. Also seen in the figure is the dynamic overshoot of stresses caused by using an applied strain rate of 4.0 x 10^4 s^{-1}.

At the larger length scales used in DD simulation, similar grain size dependent behavior is observed compared to MD analysis results. For the same dislocation density, larger grain dimensions allow increased glide of dislocations thus enhancing a d uctile material response. Smaller grains require higher internal stresses to maintain stable dislocation loops and,

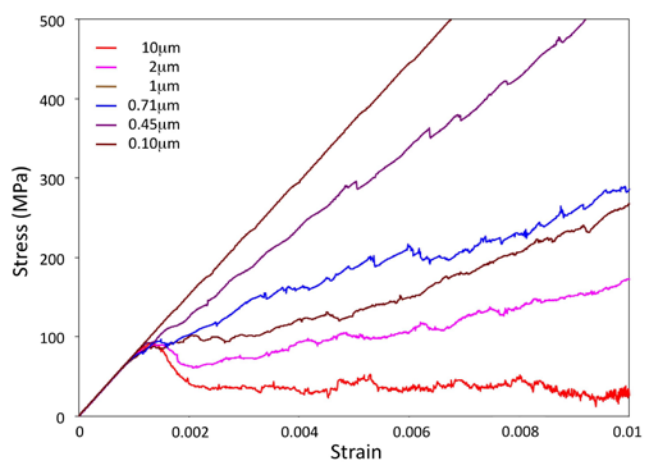

Figure 34. Stress-strain curves of Al micro-crystalline samples.

additionally, offer less freedom for dislocation glide prior to encountering a GB, interaction with another dislocation, or encountering an obstacle, all of which result in either a pile-up or pinning. Decreased dislocation motion is the primary cause of strain hardening. It should be noted that the MD simulations discussed in Section 2 did not include bulk dislocation sources or obstacles to interfere with dislocation glide and generally demonstrated softening behavior after yield.

For grain diameters, $d \geq 100$ nm, the stress-strain behavior was shown to follow the expected direct HP relation repeated from Section 2.0 as

$$\sigma_y = \sigma_o + \frac{\alpha}{\sqrt{d}} \tag{6}$$

where σ_y is the yield stress, σ_o is regarded as the resistance of the lattice to dislocation motion, α is a strengthening coefficient, and d is the average grain diameter. Because of the dynamic stress overshoot as exhibited in Figure 34, an approach was used similar to that in the MD simulation where an "averaging window" was used located away from the initial peak stresses. For the DD simulations, the final stress at the completion of 1.0% strain loading was used as an overall measure of the constraining effects of GBs on the stress. The constraining effects where quantified through an alternate form of Equation 6 as

$$\sigma_{final} = \alpha\, d^{-\eta} \tag{7}$$

where σ_{final} is the stress at 1.0% strain and η is a fitting exponent. The magnitude of this stress measure depends on the history of dislocation interactions that includes pile-ups at GBs, dislocation nucleation and annihilation, and pinning by obstacles. The relationship between final stress and grain size predicted by DD is shown in Figure 35 and closely follows the HP relationship with an exponent of 0.51. Here, a similarity is assumed between changes in yield stress and final stress at maximum applied strain. This prediction is very close to the classically assumed HP value of 0.50 for yield stress (Hall, 1951; Petch, 1953). However, it should be noted that the validity and importance of the HP relation continues to be under debate on both experimental and theoretical grounds (Huangt, 2000); it has been observed experimentally that grain sizes in the range of 100 nm to 1 μm have exhibited exponents in different materials with a range from 1.0 to 0.5.

A similar set of square-grained monocrystals was selected with side dimensions d = 2.0 μm, 1.0 μm, 0.50 μm, and 100 nm to map DD results into CP parameters for continuum finite element analyses. The stress-strain relations predicted by the simulation are presented in Figure 36. The source strength was normally distributed around a mean value given in the literature as 27.0 MPa for Al with a standard deviation of 0.2 (See Table 1) that caused the models to exhibit an aggregate flow stress centered around 0.075% applied strain. Because dislocations are initially absent in the model, yield can only begin when this source strength is exceeded. After a source nucleates a dipole pair, it is required to remain dormant during the nucleation time of 10 ns.

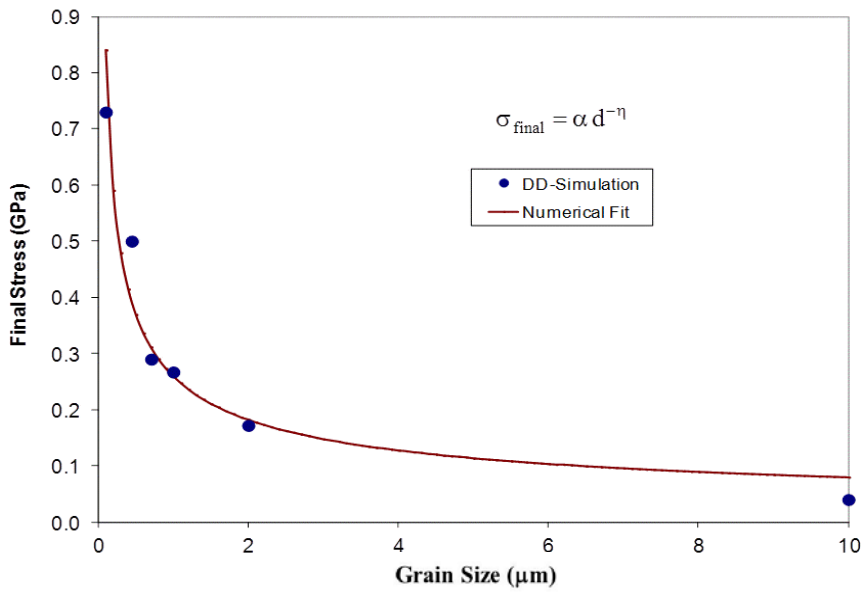

Figure 35. Dependence of final stress on grain size.

The observable trend from the DD analyses is an increasing hardening response with decreasing grain diameter. The response of the 0.1 μm grain is essentially linear-elastic for the selected source density. The 0.5 μm grain exhibits distinct episodes of slip that result in a clear nonlinearity in stress-strain behavior. For the larger, 1.0μm and 2.0μm grains, stress-strain recovery shows a linear response until the initial nucleation of dislocations from sources followed by stress relief at approximately 0.1% strain. Similar DD simulation behavior showing stress relaxation has been presented elsewhere (Deshpande, 2001; Balint, 2006). After relaxation, depending on the grain size, the stress-strain behavior either exhibits strain hardening with additional applied load or fluctuation about a constant stress indicating a state of perfect plasticity.

The stress-strain curves from the DD simulations are shown in Figure 36 together with the corresponding optimized DD/CP model predictions. The DD/CP model results for the 0.1 μm and 0.5 μm grains are indistinguishable from the corresponding DD simulations. For the larger 1.0 μm and 2.0 μm grains that demonstrate a large degree of plasticity, the optimization of the DD/CP model parameters are necessarily constrained by the number of adjustable CP parameters and the mathematical forms of the governing CP equations. The result is that the main features of the DD stress-strain relations, notably the flow stress, the slope of the hardening curve, and strain energy equal to the area under the curve, are represented in an averaged sense by the optimized DD/CP model.

5.2 Comparison of DD and CP Simulations of a Structurally-Graded Material

For simplicity, models composed of idealized square grains, as shown in Figure 37, were generated to represent the structurally-graded material. Square grains were selected to

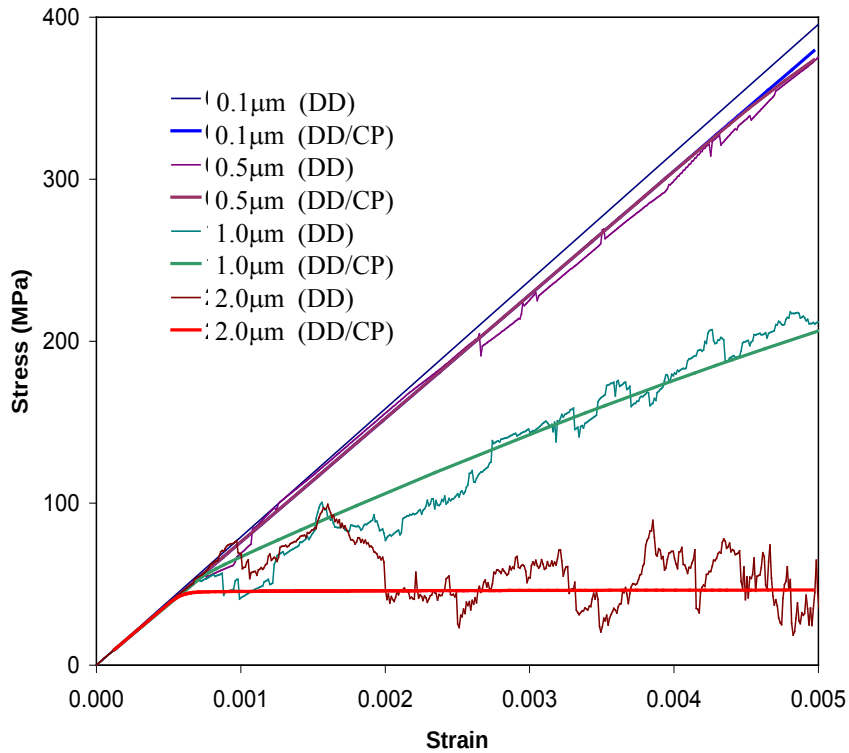

Figure 36: Comparison of stress-strain predictions using DD and the optimized DD/CP model.

carefully control grain size composition and distribution in the models. While the grain size is important for dislocation nucleation and glide, the actual shape of a grain is immaterial because the GB properties and slip system orientation are input in the two-dimensional DD analysis used herein. Previous studies using aluminum properties showed that grains with a diameter of d = 2 μm are effectively perfectly plastic while grains with d = 100 nm are essentially linearly elastic (see Figure 36). The models represent microstructures within this range of grain sizes. All grains were assumed to possess the same +60/0/-60 degree slip system. As a verification of the present approach, the configurations were simulated using both DD and the multiscale DD/CP models under uniaxial loading to 0.5% strain in the y-direction. T he DD model of the structurally-graded material was simulated using periodic boundary conditions (PBC) only in the vertical direction to remove edge effects on the top and bottom surfaces and free edge conditions on the left and right surfaces to preserve the effect of grading in the x-direction. If PBCs were introduced on the left and right surfaces, images would have been produced that would cause the smallest grains on the right to be influenced by an adjacent image of the largest grain on the left. The DD/CP model of the graded material was simulated under plane-strain conditions with CP parameters obtained using the stress-strain results of fully periodic single grain DD simulations.

For the two models investigated, the average grain size for Model 1 equals 0.7559 μm while for Model 2 equals 0.3085 μm. The GB-dislocation interactions were assumed as

'reflective' such that dislocations are prevented from crossing the GB and are free to glide back into the interior domain of the grain. The DD models are shown in Figure 37 and the corresponding continuum DD/CP finite element models are shown in Figure 38.

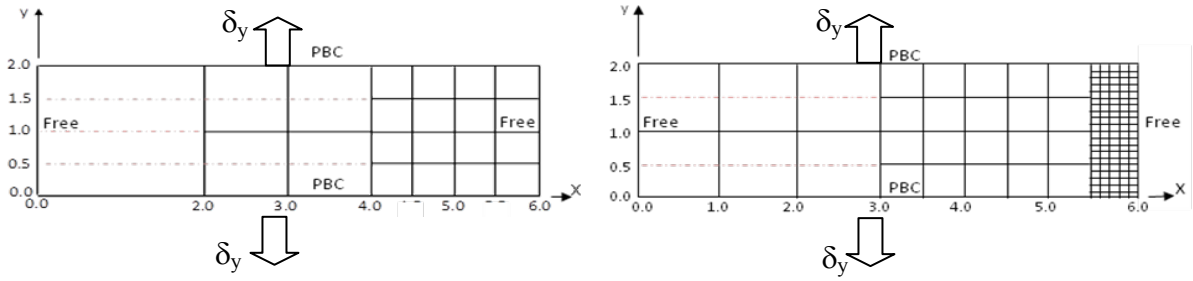

a) Model 1 b) Model 2

Figure 37: Structurally-graded polycrystal model containing 2.0μm, 1.0μm, 0.5μm and 0.1 μm square grains. Boundary conditions applied to model faces are identified as Free or PBC. All model dimensions are in microns.

Model1 Model2

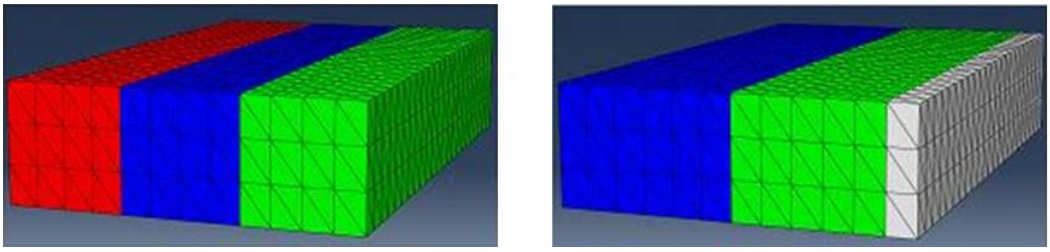

Designation of assumed grain sizes:

= 2.0μm x 2.0μm = 1.0μm x 1.0μm
= 0.5μm x 0.5μm = 0.1μm x 0.1μm

Figure 38. CP continuum models with different distributions of grain sizes.

Figure 39 shows the stress-strain results of the DD simulation and the DD/CP model. The DD simulation predicts an expected initial peak stress of about 60 MPa followed by an immediate drop in stress after which begins a steady progression of strain hardening. As seen in the figure, the DD/CP model follows the DD predictions closely up to the first peak at a stress of approximately 60 MPa and then follows a strain hardening path that is roughly parallel but somewhat offset from the DD results. An examination of Equation 5 shows that the CP hardening equation used in the DD/CP model cannot represent the localized drop in stress as predicted by the DD analysis. Thus, the discrepancy between the DD and DD/CP curves is believed to be the result of a combination of the dynamic strain rate effects in the DD simulation and the inability of the DD/CP model to represent non-monotonic hardening.

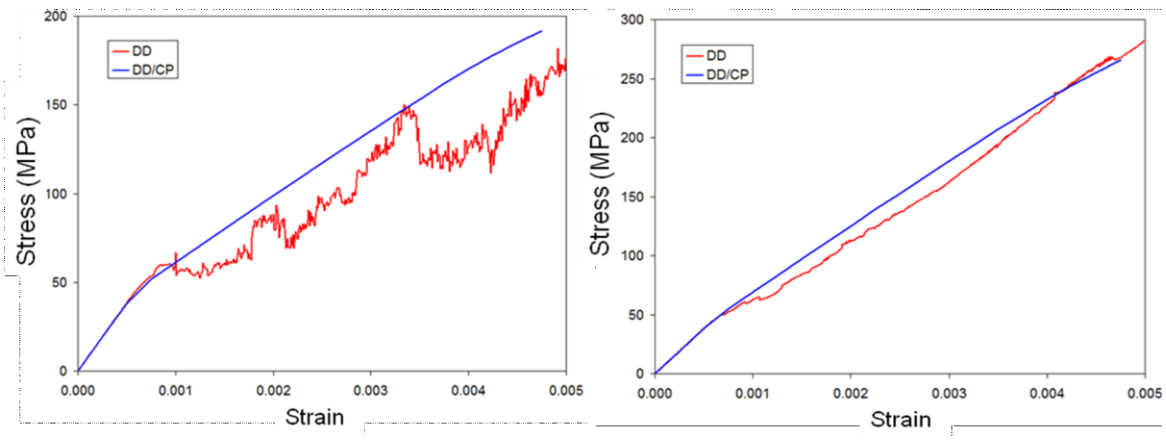

a) Model 1 b) Model 2

Figure 39. Comparison of DD and DD/CP-predicted stress-strain behavior in the structurally-graded polycrystal models.

Because of the larger proportion of smaller grains in Model 2, the DD and DD/CP analyses predict a more brittle response compared to Model 1 and, therefore, exhibit a closer agreement. For both models, good agreement is found in the replication of yield stress, slope of strain hardening, and the final stress magnitude at 0.5% strain. The reduced nonlinearity in Model 2 due to a smaller average grain size appears to be responsible for a reduction in dynamic overshoot and increased strain hardening slope compared to Model 1.

5.3 Study of Dislocation Production and Load Transfer in a Polycrystal Model

A polycrystal model generated using a Voronoi tesselation (Aurenhammer, 1991) with a highly graded microstructure is analyzed using DD. While the tessellation produced more realistic grain geometries, DD simulation does not depend on the shape of the grain because, for dislocations interacting with a GB, the GB is simply described as a line in space with assigned properties. The model consists of 197 grains with a grain aspect ratio equal to ~420 and GBs were assumed to be transmissible for dislocation passage into adjacent grains. Figure 40 shows the microstructure with an initial distribution of Frank-Read sources (blue) and GB sources (red). Point obstacles were also included to provide pinning obstructions to dislocation glide. Both source and obstacle density was selected as 7.4×10^{14} m^{-2} and represent a typical density of defects produced during fabrication. Normal loading in the y-direction was applied to 1.0% strain. For the selected model configuration, a typical stress-strain curve for the polycrystal is presented in Figure 41. The initial linear segment is identified as Stage I of the material response.

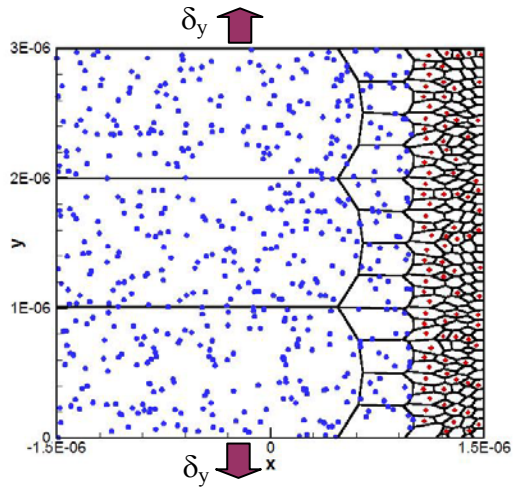

Figure 40. Graded model showing Frank-Read sources (blue) and GB sources (red).

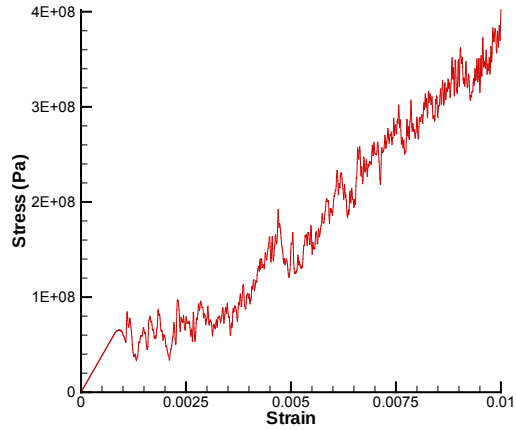

Figure 41. Typical stress-strain curve.

The initial nucleation of dislocations due to Frank-Read sources precipitates yield and begins in the larger grains. The onset of plastic flow begins Stage II of material deformation. A typical free dislocation production history is shown in Figure 42. The saw-tooth pattern is due to several effects. First, each source exhibits a 1.0 ns quiescent period during which it cannot nucleate another dislocation pair. Second, after generation, dislocation glide can cause it to pin at interior obstacles or along a GB. Finally, a dislocation can encounter another dislocation dipole of opposite sign that causes annihilation. Both the pinning and annihilation processes cause the dislocation density curve to decrease with increasing strain.

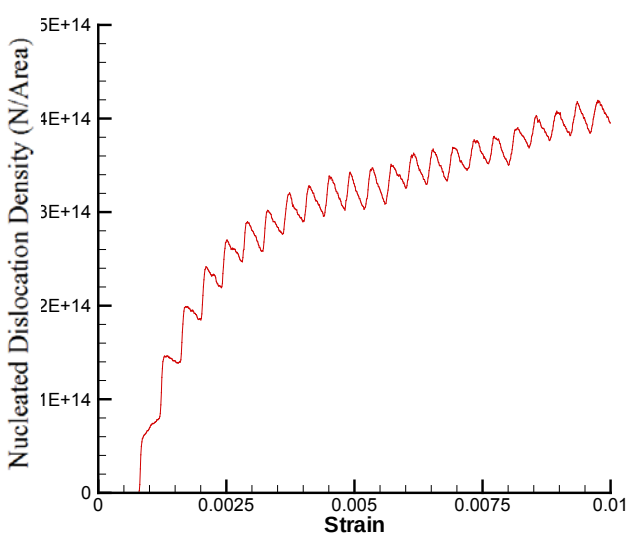

Figure 42. Nucleation of free dislocations.

At 1.0% strain, the overall model density of free dislocations shown is correlated with the strength of GB sources. As shown in Figure 43, the effect of GB nucleation strength is small because, in the 3 μm x 3 μm polycrystal model used, the small grains assigned GB sources comprised only 18.3% of the total area and were subject to increased frequency of dislocation annihilation due to the small grain size. The dislocation density shows an approximate 20% decline in dislocation production in the model with the highest GB nucleation strength.

Dislocation density profiles were generated for each simulation that show the reduction in dislocation nucleation in the smaller grains as a function of the increased GB source nucleation strength. The nanoscale size of the smaller grains generate fewer free dislocations from GB sources than the larger grains that permit Frank-Read sources to operate even starting with the same source density. The smaller grains exhibit higher energy mechanisms such as GB sliding, migration and grain rotation that are exhibited at larger applied loads.

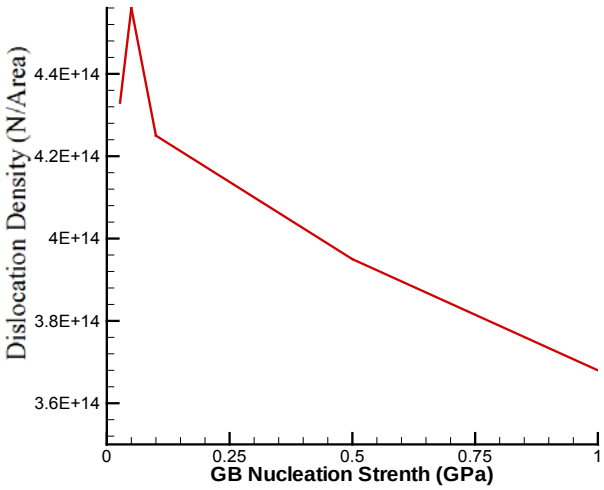

Figure 43. Final density of free dislocations at 1% strain as a function of GB strength.

For the polycrystal model depicted in Figure 40, the time evolution showing spatial dislocation density profiles at 0.2, 0.4, 0.6, 0.8 and 1.0% strains is presented in Figure 44. The contour plots are calculated over the 3 μm x 3 μm model dimensions shown in greater clarity in Figure 40. Dislocation nucleation is shown to primarily occur in the larger grains that exhibit greater ductility at lower applied loads. The general increase in dislocation density follows the increase in applied loading and repeated generation from dislocation sources over time. The present simulations were performed over 25 ms to reach full load. The important feature depicted in the density profiles is the significant reduction of dislocation production in the small grain region of the model even with increasing applied loading.

For higher GB nucleation strengths, dislocation production can cease entirely if the local stress is insufficient to cause nucleation. Figure 45 shows dislocation profiles over the model domain at 1% applied strain for GB source strengths in the range of 0.027 to 1.0 GPa. As expected, the dislocation density is highest in the small grain region when the GB nucleation strength is lowest and decreases as the strength barrier to GB dislocation production is raised.

Transgranular deformation is due to dislocation glide within grains. In the graded microstructure analyzed here, slip is dependent on both the number of dislocations present and the extent of the crystal domain over which dislocations may glide before encountering an embedded obstacle or a GB. With the grain sizes fixed, changing the GB source nucleation stress controls the number of dislocations produced within the smaller grains and affects the magnitude of slip deformation exhibited by these grains. Figure 46 shows distributions of slip magnitudes for models with GB nucleation stresses varying from 0.027 GPa to 1.0 GPa. In all simulations, the primary result is the relatively small magnitude of slip (plasticity) exhibited in the small grain region. The DD analysis performed here corroborates the assumption under Stage II deformation for a graded material that plastic flow is mostly concentrated in the larger grains in the interior while the outer small grains exhibit a primarily linear elastic response.

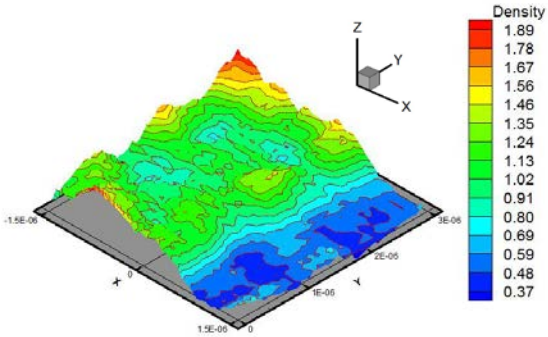

a) 0.2% strain

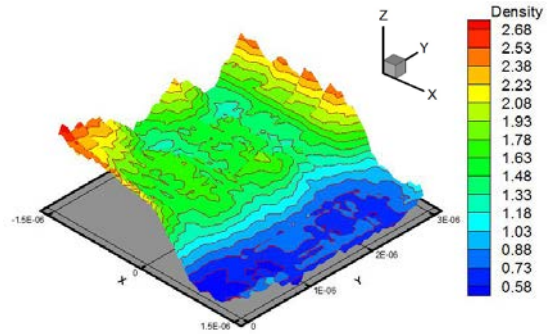

b) 0.4% strain

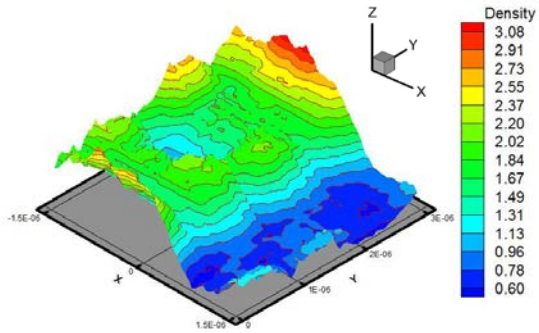

c) 0.6% strain

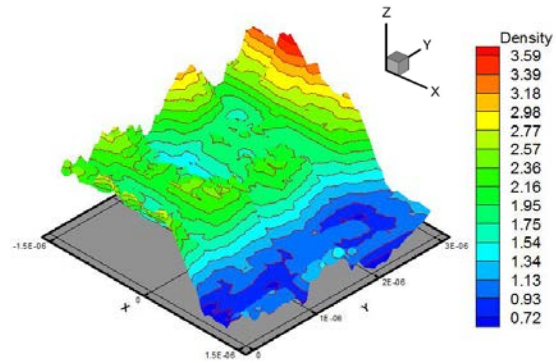

d) 0.8% strain

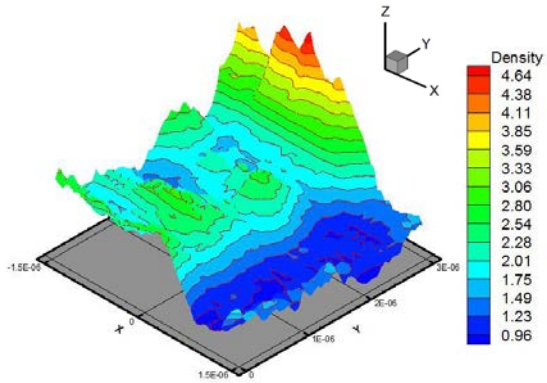

e) 1.0% strain

Figure 44. Sequential evolution of spatial dislocation density.

Figure 47 shows the averaged normal stress along the upper surface of the model at a load of 1% strain. It can be observed that the inner large grain region exhibits a reduced normal stress due to plastic yielding while the small grains in the outer region carry a higher stress due to their greater stiffness.

Thus, during Stage II, the onset of yielding and subsequent accumulation of dislocations is primarily concentrated in the core that contains the larger, ductile grains. This causes a continuous load redistribution as the outer stiffer region of the model composed of small

grains carry an increasing fraction of the applied load. This load transfer is conjectured to continue until the energy barriers to additional deformation mechanisms are exceeded which defines the transition from Stage II to Stage III deformation. The additional excited mechanisms are associated with grain boundary sliding, stress-based GB migration, and grain rotation which degrades the small grains in the outer region. The simulation of these deformation mechanisms are not possible within the analysis framework of DD but have been shown through MD simulations as discussed in Section 2.1.

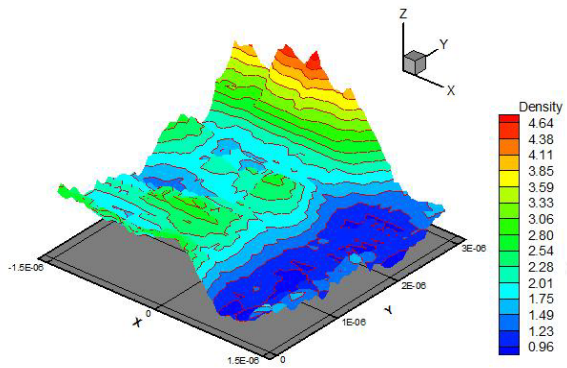

a) GB Nucleation strength = 0.027 GPa

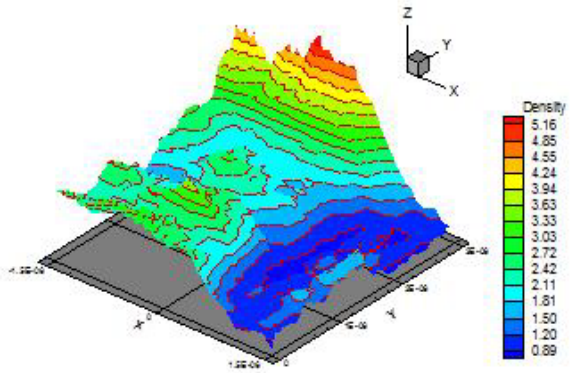

b) GB Nucleation strength = 0.05 GPa

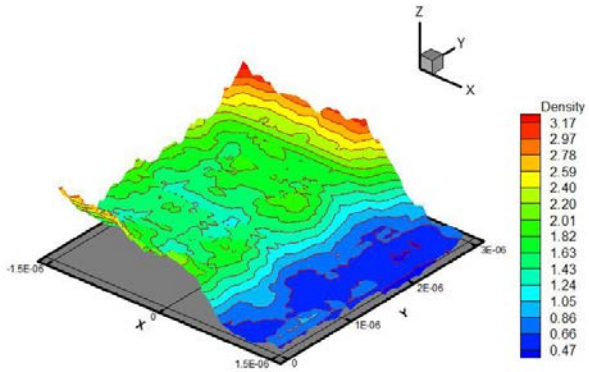

c) GB Nucleation strength = 0.1 GPa

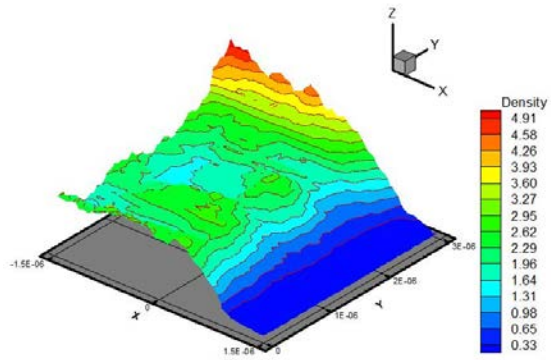

d) GB Nucleation strength = 0.5 GPa

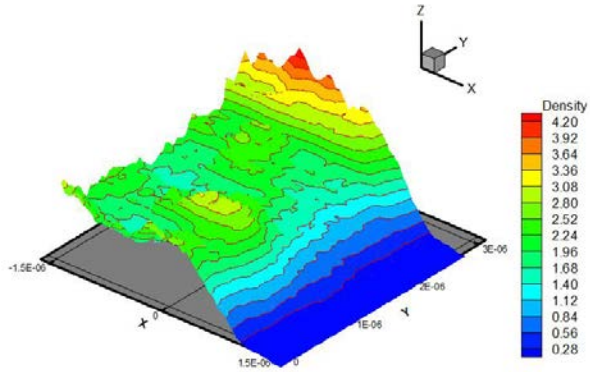

e) GB Nucleation strength = 1.0 GPa

Figure 45. Dislocation profiles at 1.0% strain as a function of GB nucleation strength.

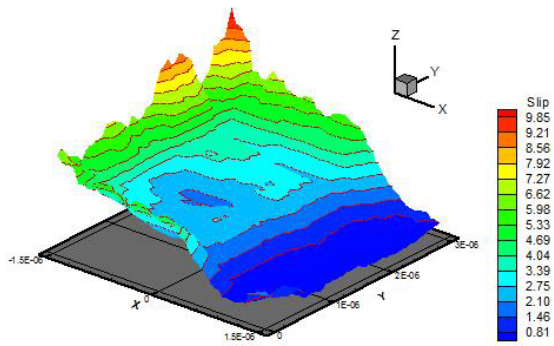

a) GB Nucleation strength = 0.027 GPa

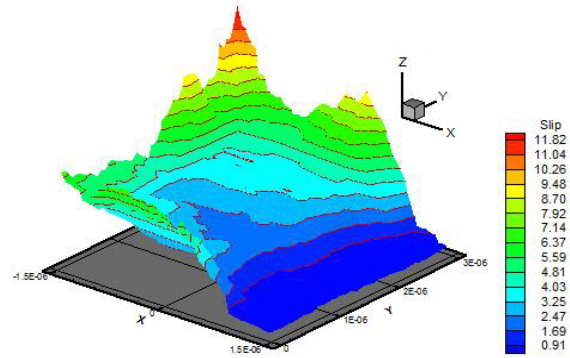

b) GB Nucleation strength = 0.05 GPa

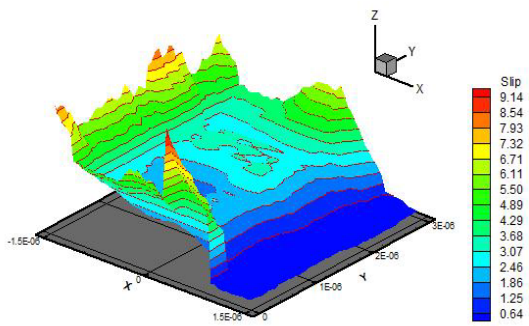

c) GB Nucleation strength = 0.1 GPa

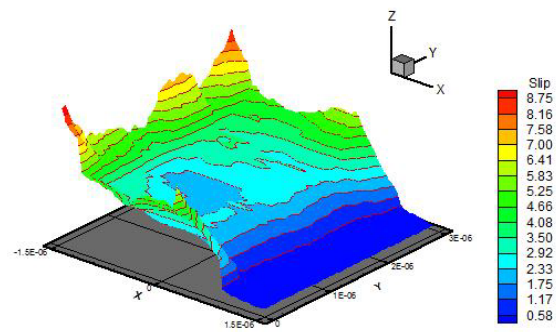

d) GB Nucleation strength = 0.5 GPa

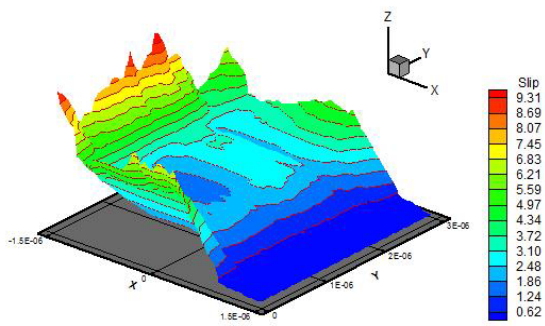

e) GB Nucleation strength = 1.0 GPa

Figure 46. Slip distribution profiles as a function of GB nucleation strength.

In general, this simulation supports the apparent failure progression during Stage II deformations presented in Section 2.1.1 in which the increase in yield strength is due to the brittle behavior of the small grains along the exterior and that the preservation of toughness is due to the plastic deformation at higher loads of the larger grains in the interior.

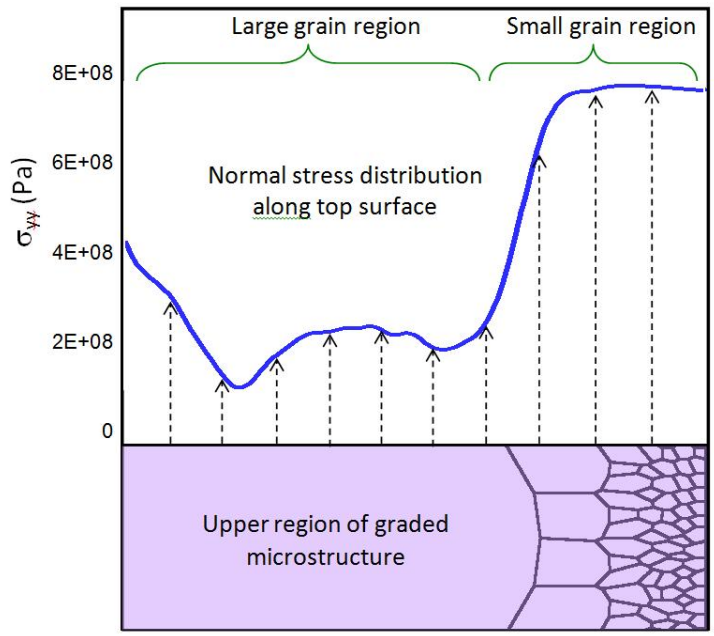

Figure 47. Variation of normal stress σ_{yy} along the upper surface.

5.4 Mapping CP Parameters using DD Simulations of Transmissible GBs

An additional set of DD simulations for CP parameter mapping was performed using a series of idealized graded polycrystal models as shown in Figure 48.

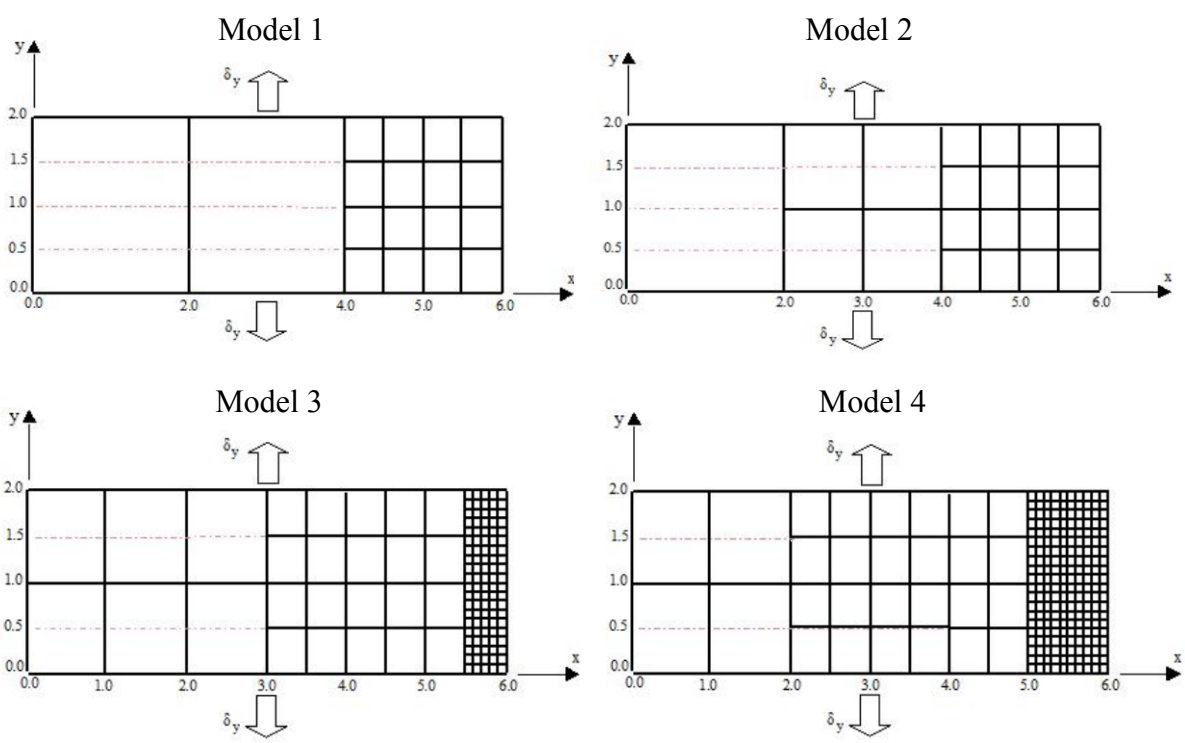

Figure 48. Polycrystal models with average grain sizes given by: Model 1 = 0.8167 μm; Model 2 = 0.7559 μm; Model 3 = 0.3085 μm; Model 4 = 0.2293 μm.

Simulations used the graded DD models with varying GB strength for transmitting dislocations. PBCs could not be applied due to the transmissible GBs behavior. While MD studies gave a 1.37 GPa strength for a Σ5 GB, DD results are obtained between 0.0 and 2.0 G Pa to interpolate effective barrier strengths for other GB orientations. The results of these simulations are presented in Figure 49.

The series of stress-strain curves show increasingly brittle behavior with decreasing grain size. For each model, decreasing the barrier strength for dislocation transmission increases ductility due to the greater freedom of mobile dislocations to undergo glide.

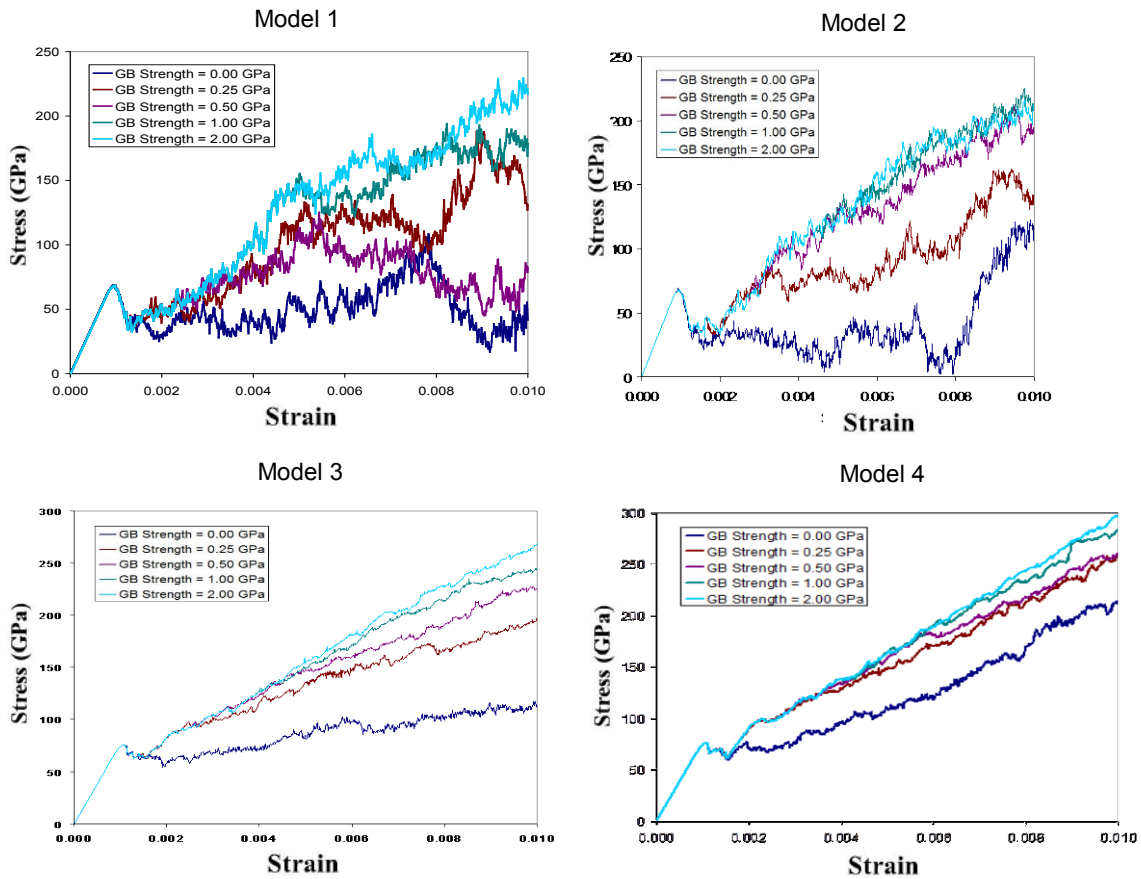

Figure 49. Stress-strain response of the four polycrystal models with variable GB strength.

Current simulations model GBs as transmittable with an energy barrier that will allow dislocations to glide into adjacent grains. No periodicity in boundary conditions was assumed. Earlier mappings of CP parameters were made to monocrystal DD simulations using reflective GB behavior and periodic boundary conditions to approximate an infinite domain. A revision of the original CP parameters using full polycrystal models and free boundary conditions was made to adjust for transmittable GB behavior. This revision was made by modifying two of the original eight CP parameters: the hardness rate parameter, G_o, and the initial hardness, g_o, which are strongly correlated with the stress-strain slope

and yield stress, respectively. In this modified parameterization, the apparent softening due to initial spurious dynamic effects was neglected in calibrating CP parameters.

The continuum DD/CP models that duplicate the cross-section geometries and grain size domains are shown in Figure 50. The resulting comparisons between DD and DD/CP stress-strain predictions are shown in Figure 51. The DD results exhibit an increased fluctuation of stresses for larger grains. The resulting stress-strain predictions compare reasonably well between DD and CP analyses.

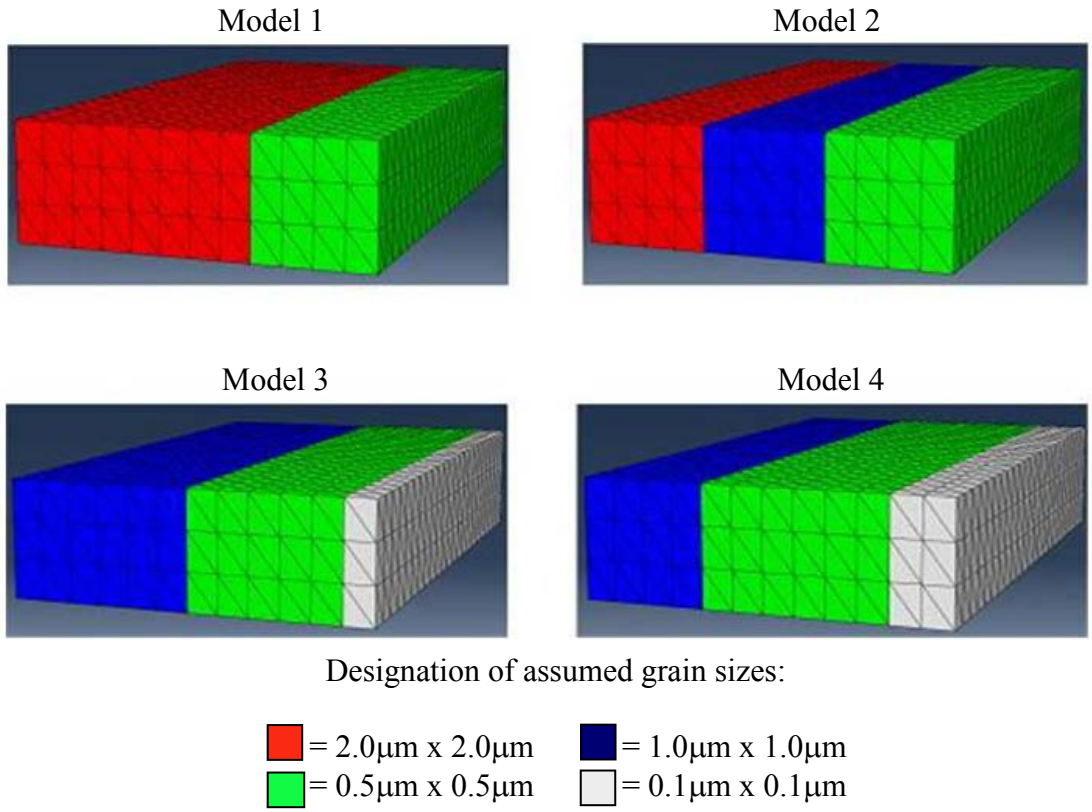

Figure 50. CP continuum models with different distributions of grain sizes.

Comparing different assumed GB – dislocation interactions, the PBCs used for reflective GB behavior provided a procedure for obtaining grain properties that rigorously accounted for infinite material domains. For transmissible GBs, PBCs could not be used as boundary conditions and, thus, the grains had to be simulated with free boundary conditions. It was determined that the different GB-dislocation behavior did not have a large effect in determining effective CP parameters. There is, however, a general theoretical question about determining CP parameters using monocyrstal DD simulations. This issue involves the long-range influence of stress fields associated with dislocations and the degree of inaccuracy when using monocrystal-derived CP parameters in a model that has small and large grains in close proximity. One would expect a large influence that would not be captured by individual DD simulations yet, in comparing the stress-strain curves for polycrystal models using purely DD and DD/CP anaysis frameworks, the results were very similar.

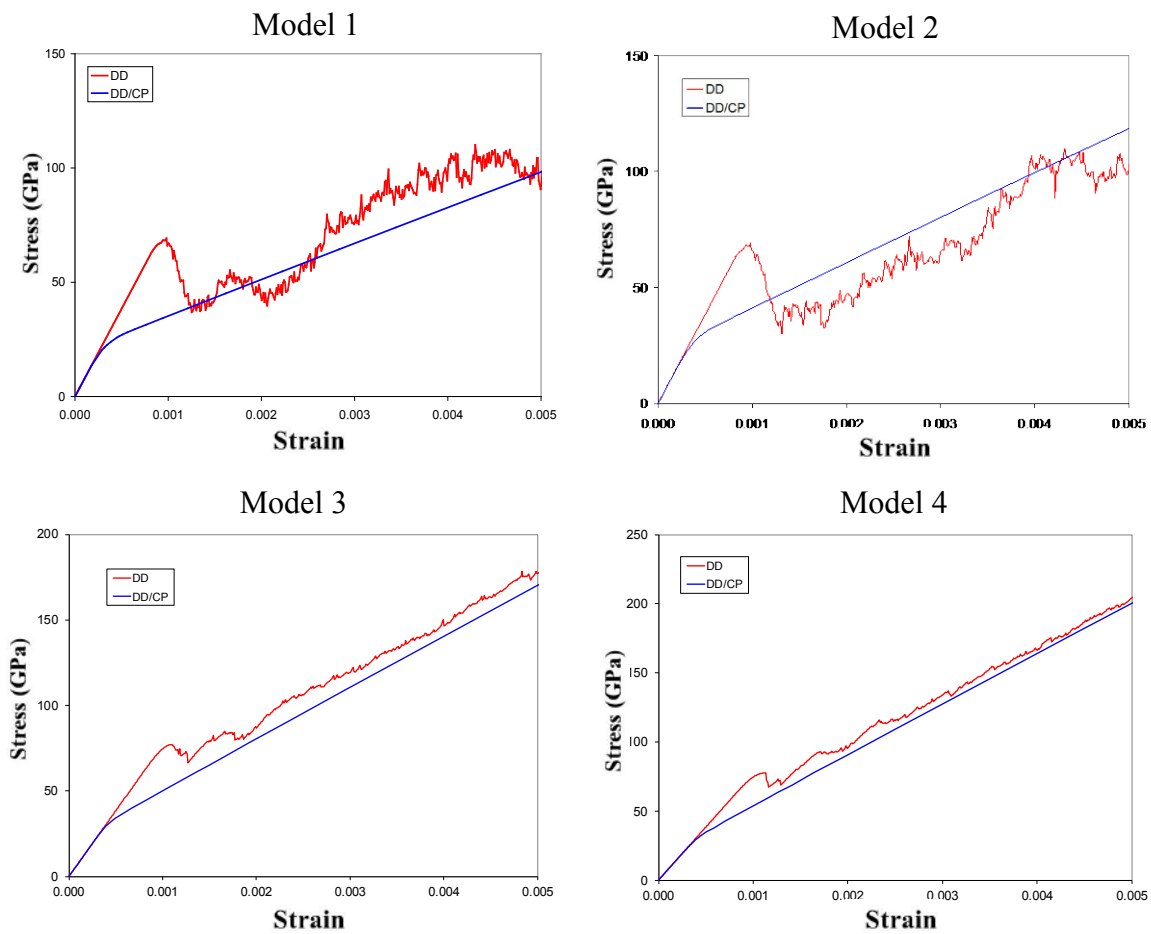

Figure 51. Comparison of stress-strain predictions using DD and calibrated CP analyses.

5.5 Study of Strain Rate Effects

Figure 52 shows a parametric study of applied strain rates in DD analyses on the stress-strain curves generated for the polycrystal model that shows the overshoot reducing with decreasing strain rate. Here, trendlines were computed to smooth out the data for each applied strain rate. The lowest strain rate applied was 1000 s^{-1} which is, however, at a time increment that is impractical for use in a complete simulation due to excessive computer run-times.

Using DD, this local peak after initial yield has been observed by other authors (see, for example, Despande, 2001; Balint, 2006) and is believed to occur because the applied strain rate of 4.0×10^4 s^{-1} in the DD simulation does not allow sufficiently rapid dislocation nucleation to immediately soften the material. This overshoot was also observed in MD analysis and described in Section 2.0.

The plot in Figure 53 shows stress-strain and dislocation generation data for the polycrystal model in the region of stress overshoot where the applied strain was ramped at a rate of 4 x 10^4 s^{-1}. Stresses and dislocations were normalized to peak values attained at an applied strain of 0.01. The overshoot proceeds through an initial peak stress and stress relaxation after an applied strain of ~0.125 after which strain hardening is manifest and stresses begin to monotonically increase thereafter. Dislocation nucleation starts when the applied stress reaches the source strength of 0.27 GPa. The steady accumulation of dislocations while stresses continue to increase with applied strain supports the hypothesis that the overshoot is partly due to the lag in dislocation production that allows stresses to increase before being counteracted by dislocation stress fields. Further study is warranted to investigate ways to ameliorate this dynamic effect that could involve imposing dwell times during the initial phase of dislocation nucleation, implementing faster computational procedures such as multipole expansion methods (Greengard, 1990), or utilizing parallel processing to permit slower strain rates to be applied to large systems of dislocations.

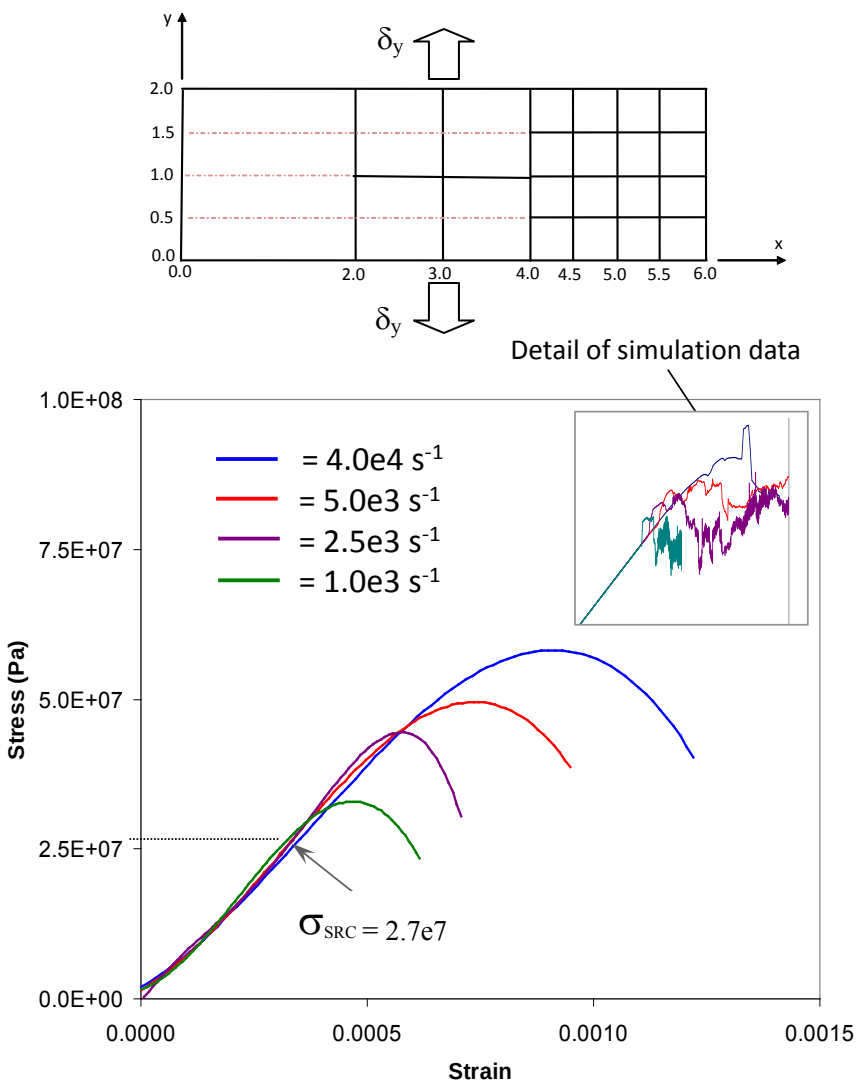

Figure 52. Magnitude of stress overshoot with applied strain rate.

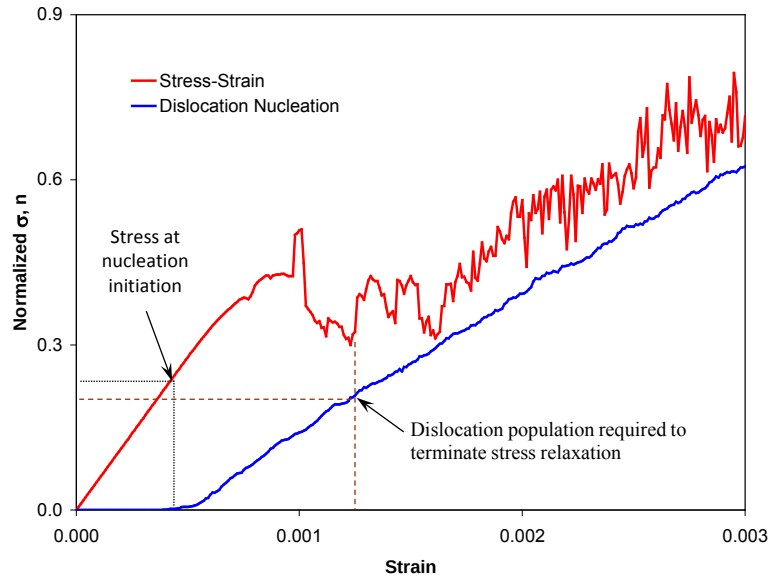

Figure 53. Stress overshoot as a function of dislocation nucleation.

6.0 Simulation of Macroscopic Models Containing Graded Microstructures

A single cylindrical dogbone model possessing a radially graded microstructure was presented by Fang (Fang, 2011) where a depiction of the specimen and representation of the structurally-graded microstructure are repeated from Figure 1 for convenience in Figure 54. This specimen was fabricated using Cu with a grain distribution presented in Figure 55. Experimental tests demonstrated improved material response by exhibiting a significant increase in yield stress while preserving ductility as presented in Figure 56.

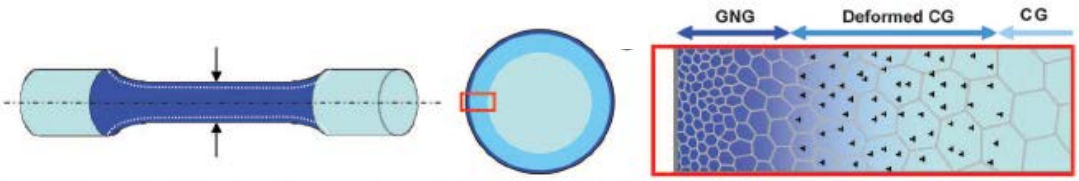

Figure 54. Cylindrical dogbone specimen with graded microstructure.

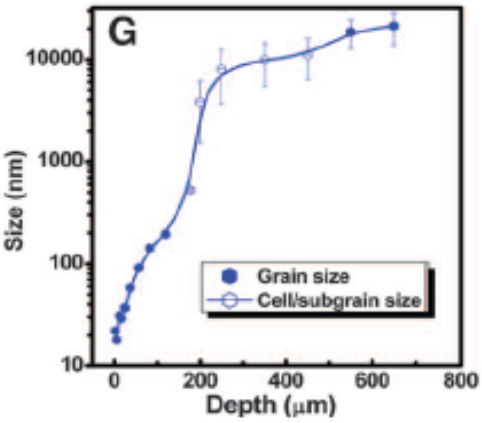

Figure 55. Grain diameter with depth.

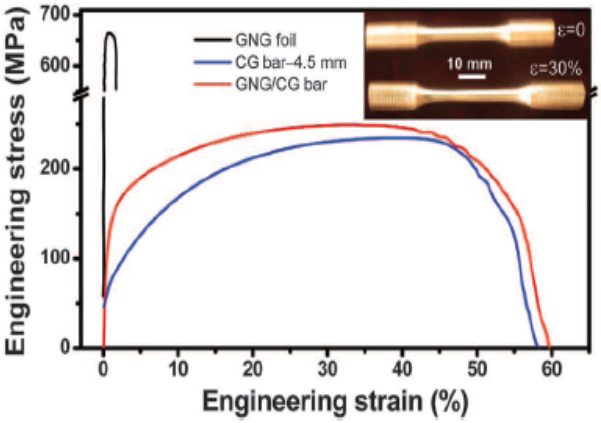

Figure 56. Stress strain behavior of graded material to ultimate failure.

Multiscale analysis allows the simulation of specimen geometry large enough to be experimentally accessible. The specimen dimensions are given in Figure 57. A profile of the dogbone specimen including the grip and test sections is shown in Figure 58. Figure 59 shows the two planes of symmetry exploited in the DD/CP model to reduce the number of active degrees of freedom, and the cylindrical grading pattern configuration of the microstructure.

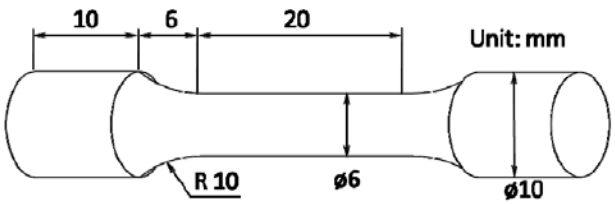

Figure 57. Tensile bar geometry. (From Fang, 2011)

Simulations were performed on Al cylindrical models composed of entirely nanoscale grains (d = 100 nm), entirely coarse grains (d = 2 μm), and concentric layer configurations containing different grain sizes to represent a graded microstructure (d = 100 nm - 2 μm). The simulations were limited to a small applied strain because the strain softening associated with grain rotation and grain boundary migration at higher strain levels leading to final failure cannot be represented in a DD or CP framework.

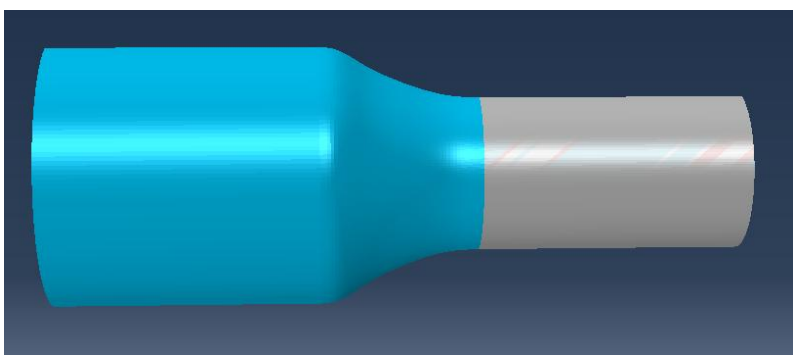

Figure 58. Axial profile of grip and test sections.

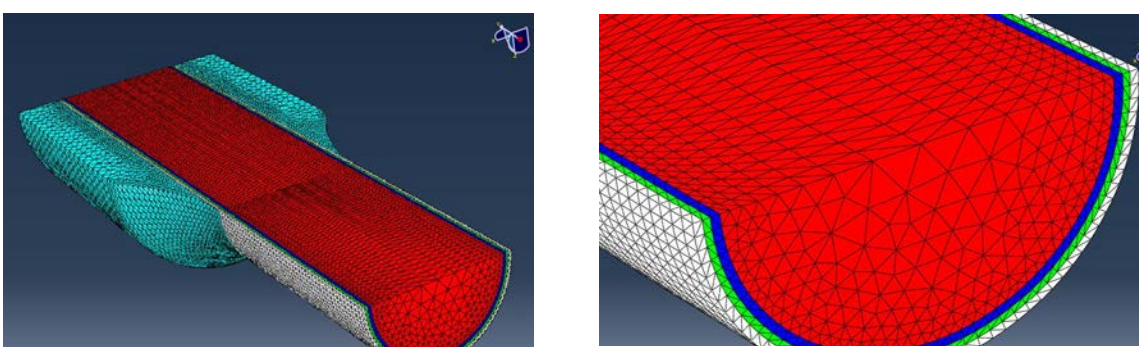

a) Symmetry planes used in model. b) Detail of the graded microstructure.

Designation of assumed grain sizes:

= 2.0μm x 2.0μm = 1.0μm x 1.0μm
= 0.5μm x 0.5μm = 0.1μm x 0.1μm

Figure 59. Finite element model of graded cylindrical dogbone specimen.

To assess the effect of microstructure on yield stress and overall stress-strain response, three different models were generated with different microstructural configurations. As shown in Figure 60, the models differ in the relative thickness of the concentric layers containing grains of different size. The grain size as a function of depth is contained in separate graphs.

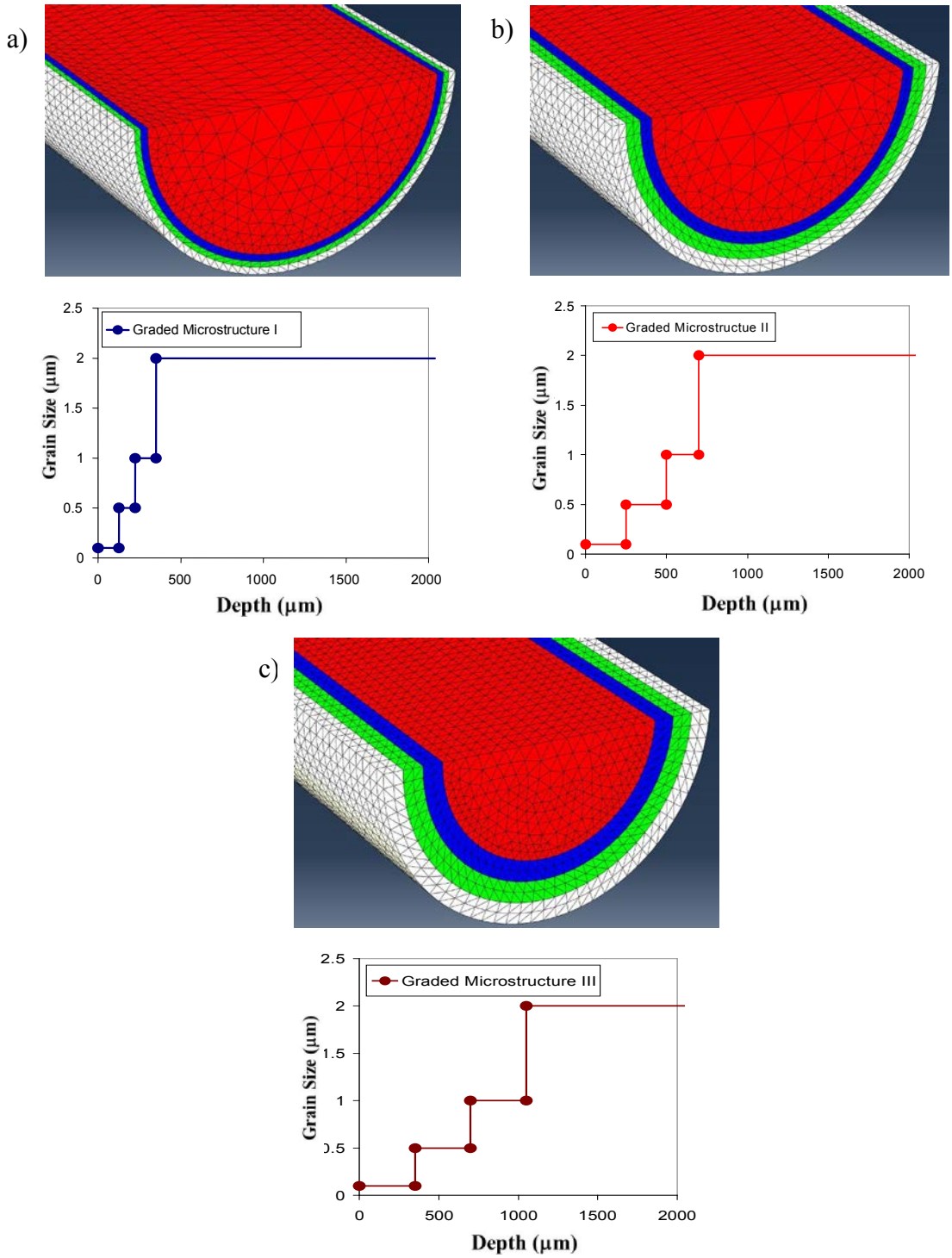

Figure 60. Cross sections depicting a) Microstructure I, b) Microstructure II, and c) Microstructure III.

Changing the relative volume fraction of differently sized grains results in an inverse relationship in which increasing the relative size of small grained regions increase the material yield stress while decreasing the overall ductility. Thus by changing the material architecture, a tailoring of properties is possible to optimize materials for specific service applications. In the present study, a qualitative comparison between the multiscale simulations of the different Al models show a similar trend in increased yield stress and preserved ductility with microstructural grading as was demonstrated by Fang (Fang, 2011) in experiments using Cu specimens. This comparison is presented in Figure 61.

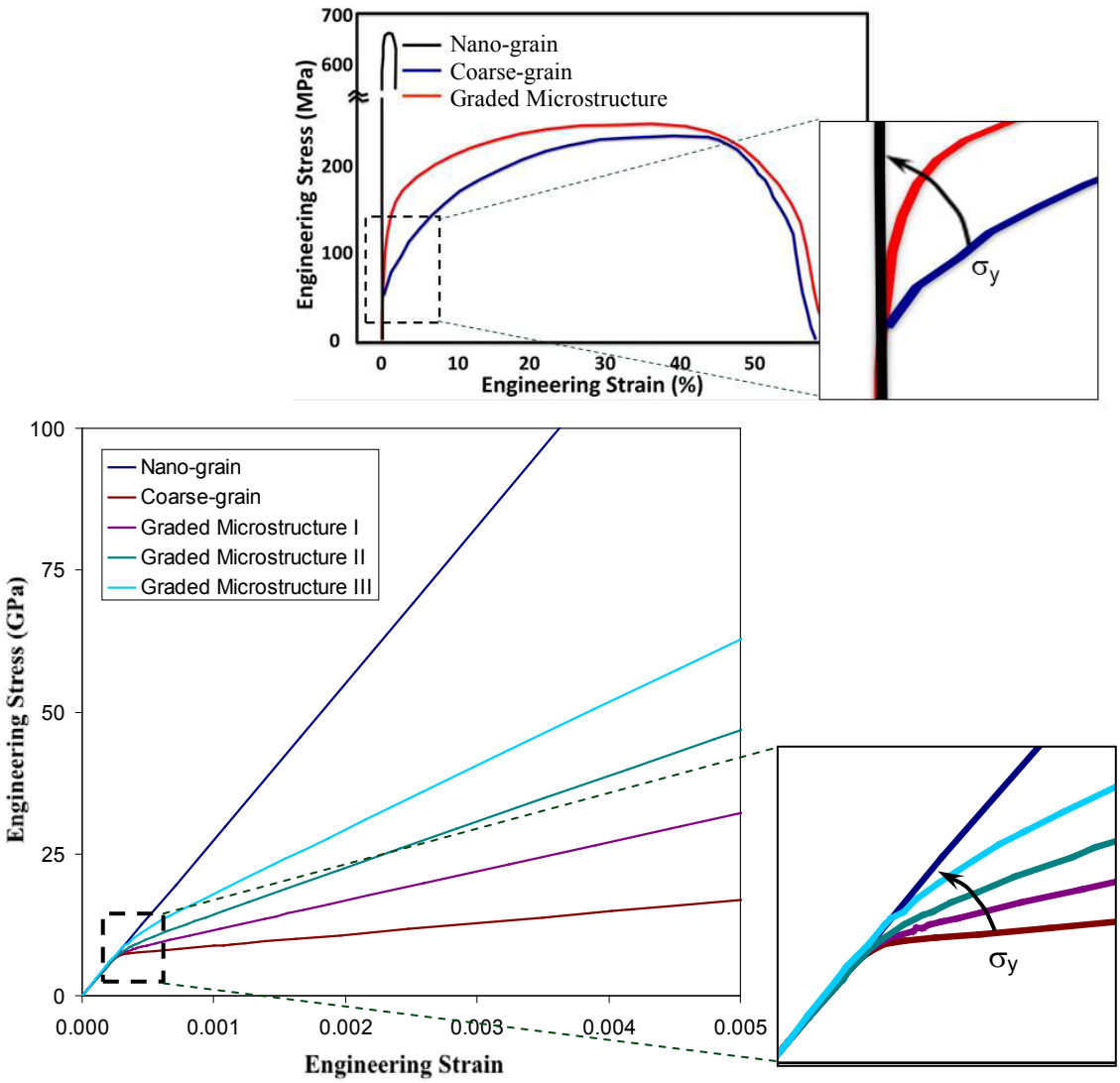

Figure 61. Qualitative comparison between experimental data for a Cu dogbone specimen and current simulation results for an aluminum specimen using the developed multiscale analysis approach.

7.0 Summary

A multiscale modeling method has been developed that links simulation results using MD, DD and CP methods. MD modeling was used to study basic material failure processes and GB strength in both uniform and graded microstructures. Because MD is resolved at the atomistic level, material domains were necessarily limited in size to an upper limit of approximately 100 million atoms and simulation times were restricted to some tens of nanoseconds for practical analysis. DD simulations were performed at micron length scales to determine yield stress and strain hardening rates. The DD models used herein were limited to small structurally-graded Al materials having grain sizes that ranged from 100 nm to 2.0 μm. The results of DD analyses were then mapped into a set of effective CP parameters to permit continuum finite element analyses of domains with arbitrary size.

The study of atomistic damage mechanisms suggested that the mechanical benefits of the microstructural grading used in the present study involve two fundamental processes. One process consists of transferring load away from the interior ductile region to the stiffer outer layers that delays dislocation production causing an increase in yield stress. A second process involves delaying strain localization until higher loads are reached at which GB mechanisms such as sliding and grain rotation are initiated and diminish the load carrying capability of the stiff outer layers that evens out the internal stresses through the cross section. With this redistribution, ductile deformation in the interior increases such that shear band formation and necking are precipitated and extend through the cross section leading to ultimate failure.

A discussion of two-dimensional DD methods was presented together with their application to the study of the effects of grain size on yield stress and hardening. The effect of grain size was demonstrated by showing HP behavior by comparing stress levels at maximum applied strains. Stress-strain predictions of models containing small 100 nm grains were shown to exhibit an effectively linear-elastic response while models composed of large 2.0 μm grains demonstrated a near perfectly plastic response. This prediction was used to bound the range of grain sizes used in illustrative polycrystal models.

The optimization procedure used to calibrate CP hardening parameters and develop a dislocation-based crystal plasticity model (the DD/CP model) from the DD simulations was outlined. The main features of the DD stress-strain relations were represented in an averaged sense by the optimized DD/CP model. The stress-strain behavior of a structurally-graded polycrystal was presented comparing DD and DD/CP model results. The correspondence of the resulting stress-strain predictions was found to be good.

The calibrated DD/CP parameters permitted the modeling of macroscopic graded cylindrical models with an axial length of 52 mm and diameter of 10 mm. The size of this model is orders of magnitude greater than what could be simulated by MD or DD methods alone. These dimensions are large enough to be directly accessible to

experimental investigation. Several variations of the radially graded microstructure were simulated and showed a good qualitative agreement of the increase in yield stress between a simulated Al specimen and experimental data generated for a Cu specimen of the same geometry.

Important results from the present study have been to elucidate the apparent failure mechanisms involved in the improved material response of the radially graded material microstructure, and to develop a multiscale analysis procedure to simulate the behavior of present and future novel microstructural concepts. New classes of metallic materials containing structurally-graded microstructures offer the promise of significant improvements in strength, ductility and toughness. If graded nanocrystalline structural components can be fabricated in widely used structural materials such as Al, the improvement of aerospace vehicle weight, durability and safety metrics may be enormous.

References

1. Abuzaid, W., Sangid, M.D., Sehitoglu, H., Carroll, J., and Lambros, J., "Slip Transfer and Plastic Strain Accumulation Across Grain Boundaries in Hastelloy X," *J. Mech. Phys. Solids,* Vol. 60, 2012, pp. 1201-1220.
2. Adams, J.B., Wolfer, W.G., and Foiles, S.M., "Elastic Properties of Grain Boundaries in Copper and Their Relationship to Bulk Elastic Constants," *Phys. Rev. B*, Vol. 40, 1989, pp. 9479-9484.
3. Aurenhammer, F., "Voronoi Diagrams – A Survey of a Fundamental Geometric Data Structure," *ACM Computing Surveys*, Vol. 23, 1991, pp. 345–405.
4. Benzerga, A.A., Brechet, Y., Needleman, A. and Van der Giessen, E., "Incorporating Three-Dimensional Mechanisms into Two-Dimensional Dislocation Dynamics," *Modell. Simul. Mater. Sci. Eng.*, Vol. 12, 2004, pp.159-196.
5. Balint, D.S., Deshpande, V.S., Needleman, A., and Van der Giessen, E., "Size Effects in Uniaxial Deformation of Single and Polycrystals: A Discrete Dislocation Plasticity Analysis," *Modell. Simul. Mater. Sci. Eng.*, Vol. 14, 2006, pp. 409-423.
6. Clark, W.A.T., Wagoner, R.H., Shen, Z.Y., Lee, T.C., Robertson, I.M., and Birnbaum, H.K., "On the Criteria for Slip Transmission Across Interfaces in Polycrystals," *Scripta Metall. Mater.*, Vol. 26, 1992, pp. 203-206.
7. Deshpande, V.S., Needleman, A., and Van der Giessen, E., "Discrete Dislocation Plasticity Modeling of Short Cracks in Single Crystals," *Acta Mater.*, Vol. 51, 2003, pp. 1-15.
8. Devincre, B., Kubin, L.P., Lemarchand, C., and Madec, R., "Mesoscopic Simulations of Plastic Deformation," *Mat. Sci. Eng.*, Vol. A309-310, 2001, pp. 211-219.
9. DOT library, ref[http://www.vrand.com/DOT.html]
10. Evans, A.G., and Hutchinson, J.W., "A Critical Assessment of Theories of Strain Gradient Plasticity," *Acta Mater.*, Vol. 57, 2009, pp. 1675-1688.
11. Evers, L.P., Parks, D.M., Brekelmans, W.A.M., and Geers, M.G.D., "Crystal Plasticity Model with Enhanced Hardening by Geometrically Necessary Dislocation Accumulation," *J. Mech. Phys. Solids*, Vol. 50, 2002, pp. 2403-2424.

12. Fang, T.H., Li, W.L., Tao, N.R., and Lu, K., "Revealing Extraordinary Intrinsic Tensile Plasticity in Gradient Nano-Grained Copper," *Science*, Vol. 331, 2011, pp. 1587-1590.
13. Fleck, N.A., Muller, G.M., Ashby, M.F., and Hutchinson, J.W., "Strain Gradient Plasticity: Theory and Experiment," *Acta Metall. Mater.*, Vol. 42, 1994, pp. 475-487.
14. Fleck, N.A., and Hutchinson, J.W., "Strain Gradient Plasticity," *Adv. in Appl. Mech.*, Vol. 33, 1997, pp. 295-361.
15. Freidman, L.H. and Chrzan, D.C., "Scaling Theory of the Hall-Petch Relation for Multilayers," *Phys. Rev. Lett.*, Vol. 81, 1998, pp. 2715-2718.
16. Gavriljuk, V.G., Berns, H., Escher, C., Glavatskaya, N.I., Sozinov, A., and Petrov, Y.N., "Grain Boundary Strengthening in Austenitic Nitrogen Steels," *Mat. Sci. Eng.*, Vol. 271, 1999, pp. 14-21.
17. Gleiter, H., "Nanocrystalline Materials," *Prog. Matl. Sci.*, Vol. 33, 1989, pp. 223-315.
18. Greengard, L. "The Numerical Solution of the N-body Problem," *Comp. Phys.*, Vol. 4, 1990, pp. 142–152.
19. Hall, E.O., "The Deformation and Ageing of Mild Steel: III Discussion of Results," *Proc. Phys. Soc.*, Ser. B, Vol. 64, 1951, pp. 747-753.
20. Han, C.-S., Gao, H., Huang, Y., and Nix, W., "Mechanism-Based Strain Gradient Crystal Plasticity-I. Theory," *J. Mech. Phys. Solids*, Vol. 53, 2005, pp. 1188-1203.
21. Han, C.-S., Gao, H., Huang, Y., and Nix, W., "Mechanism-Based Strain Gradient Crystal Plasticity-II. Analysis," *J. Mech. Phys. Solids*, Vol. 53, 2005, pp. 1204-1222.
22. Huangt, H., and Spaepens, F., "Tensile Testing of Free-Standing Cu, Ag and Al Thin Films and Ag/Cu Multilayers," *Acta Mater*., Vol. 48, 2000, pp. 3261-3269.
23. Hull, D. and Bacon, D.J., *Introduction to Dislocations*, Butterworth-Heinemann, Oxford, 2001.
24. Hutchinson, J.W., "Plasticity at the Micron Scale," *Int. J. Solids and Struct.*, Vol. 37, 2000, pp. 225-238.
25. Li, J.C.M., and Cho, Y.T., "The Role of Dislocations in the Flow Stress-Grain Size Relationships," *Metall. Trans.*, Vol. 1, 1970, pp. 1145–1159.
26. Matouš, K., and Maniatty, A.M., "Finite Element Formulation for Modeling Large Deformations in Elasto-Viscoplastic Polycrystals," *Int. J. Num. Meth. Engrg.*, Vol. 60, 2004, pp. 2313-2333.
27. Miller, R.E., Shilkrot, L.E., and Curtin, W.A., "Coupled Atomistics and Discrete Dislocation Plasticity Simulation of Nanoindentation into Single Crystal Thin Films," *Acta Mater.*, Vol. 52, 2004, pp. 271-284.
28. Mishin, Y., Farkas, D., Mehl, M.J., Papaconstantopoulos, D.A., "Interatomic potentials for monoatomic metals from experimental data and ab initio calculations," *Phys. Rev. B*, Vol. 59, 1999, pp. 3393-3407.
29. Mughrabi, H., "Dislocation Wall and Cell Structures and Long-Range Internal Stresses in Deformed Metal Crystal," *Acta Metall.*, Vol. 31, 1983, pp. 1367-1379.
30. NASA/Pleiades, http://www.nas.nasa.gov/hecc/resources/pleiades.html, 2013.
31. Needleman, A., and Van der Giessen, E., "Micromechanics of Fracture: Connecting Physics to Engineering," *MRS Bulletin*, March 2001, pp. 211-214.
32. Petch, N.J., "The Cleavage Strength of Polycristals," *Iron and Steel Institute*, 1953, pp. 25-28.

33. Roters, F., Eisenlohr, P., Hantcherli, L., Tjahjanto, D.D., Bieler, T.R., and Raabe, D., "Overview of Constitutive Laws, Kinematics, Homogenization and Multiscale Methods in Crystal Plasticity Finite-Element Modeling: Theory, Experiments, Applications," *Acta Mater.*, Vol. 58, 2010, pp. 1152-1211.
34. Saether, E., Yamakov, V., Phillips, D.R., and Glaessgen, E.H., "An Overview of the State of the Art in Atomistic and Multiscale Simulation of Fracture," NASA TM-2009-215564, 2009.
35. Schiotz, J., Vegge, T., Di Tolla, F.D., and Jacobsen, K.W., "Atomic-Scale Simulations of the Mechanical Deformation of Nanocrystalline Metals," *Phys. Rev. B*, Vol. 60, 1999, pp. 11971-11983.
36. Shen, Z., Wagoner, R.H., and Clark, W.A.T., "Dislocation and Grain Boundary Interactions in Metals," *Acta Metall*., Vol. 36, 1988, pp. 3231-3242.
37. Thomson, R., Levine, L.E., Shim, Y., Savage, M.F., and Kramer, D.E., "A Multi-Scale Theoretical Scheme for Metal Deformation," *Comp. Model. Engr. Sci.*, Vol. 3, 2002, pp. 245-253.
38. Uchic, M.D., Shade, P.A., and Dimiduk, D.M., "Plasticity of Micrometer-Scale Single Crystal in Compression," *Ann. Rev. Mater. Res.*, Vol. 39, 2009, pp. 361-386.
39. Van der Giessen, E., and Needleman, A., "Discrete Dislocation Plasticity: A Simple Planar Model," *Modell. Simul. Mater. Sci. Eng.*, Vol. 3, 1995, pp. 689-735.
40. Warner, D. H., Curtin, W. A., and Qu, S., "Rate Dependence of Crack-Tip Processes Predicts Twinning Trends in f.c.c. Metals," *Nature Mater.*, Vol. 6, 2007, pp. 876-880.
41. Whang, S.H., *Nanostructured Metals and Alloys: Processing, Microstructure, Mechanical Properties and Applications*, Woodhead Publishing, Oxford, 2011.
42. Wolf, D. and Jaszczak, J.A., "Tailored Elastic Behavior of Multilayers through Controlled Interface Structure," *J. Computer-Aided Design*, Vol. 1, 1993, pp. 111-148.
43. Yamakov, V., Saether, E., Phillips, D. R., and Glaessgen, E. H., "Molecular-Dynamics Simulation-Based Cohesive Zone Representation of Intergranular Fracture Processes in Aluminum," *J. Mech. Phys. Solids*, Vol. 54, 2006, pp. 1899-1928.
44. Yamakov, V., Saether, E., and Glaessgen, E.H., "A Continuum-Atomistic Analysis of Transgranular Crack Propagation in Aluminum," 50th AIAA/ASME/ASCE/AHS/ASC Structures, Structural Dynamics and Materials Conference and Exhibit, Palm Springs, CA, 2009.
45. Zhu, B., Asaro, R.J., Krysl, P., Zhang, K., and Weertman, J.R., "Effects of Grain Size Distribution on the Mechanical Response of Nanocrystalline Metals: Part II," *Acta Mater.*, Vol. 54, 2006, pp. 3307-3320.
46. Zimmerman, J.A., Kelchner, C.L., Klein, P.A., Hamilton, J.C., and Foiles, S.M., "Surface Step Effects on Nanoindentation," *Phys. Rev. Lett.*, Vol. 87, 2001, p. 165507.

REPORT DOCUMENTATION PAGE

Form Approved
OMB No. 0704-0188

The public reporting burden for this collection of information is estimated to average 1 hour per response, including the time for reviewing instructions, searching existing data sources, gathering and maintaining the data needed, and completing and reviewing the collection of information. Send comments regarding this burden estimate or any other aspect of this collection of information, including suggestions for reducing this burden, to Department of Defense, Washington Headquarters Services, Directorate for Information Operations and Reports (0704-0188), 1215 Jefferson Davis Highway, Suite 1204, Arlington, VA 22202-4302. Respondents should be aware that notwithstanding any other provision of law, no person shall be subject to any penalty for failing to comply with a collection of information if it does not display a currently valid OMB control number.
PLEASE DO NOT RETURN YOUR FORM TO THE ABOVE ADDRESS.

1. REPORT DATE *(DD-MM-YYYY)*
01- 05 - 2014

2. REPORT TYPE
Technical Memorandum

3. DATES COVERED *(From - To)*

4. TITLE AND SUBTITLE

Multiscale Analysis of Structurally-Graded Microstructures Using Molecular Dynamics, Discrete Dislocation Dynamics and Continuum Crystal Plasticity

5a. CONTRACT NUMBER

5b. GRANT NUMBER

5c. PROGRAM ELEMENT NUMBER

6. AUTHOR(S)

Saether, Erik; Hochhalter, Jacob D.; Glaessgen, Edward H.; Yuri, Mishin

5d. PROJECT NUMBER

5e. TASK NUMBER

5f. WORK UNIT NUMBER
432938.11.01.07.43.40.09

7. PERFORMING ORGANIZATION NAME(S) AND ADDRESS(ES)
NASA Langley Research Center
Hampton, VA 23681-2199

8. PERFORMING ORGANIZATION REPORT NUMBER
L-20410

9. SPONSORING/MONITORING AGENCY NAME(S) AND ADDRESS(ES)
National Aeronautics and Space Administration
Washington, DC 20546-0001

10. SPONSOR/MONITOR'S ACRONYM(S)
NASA

11. SPONSOR/MONITOR'S REPORT NUMBER(S)
NASA/TM-2014-218265

12. DISTRIBUTION/AVAILABILITY STATEMENT
Unclassified - Unlimited
Subject Category 27
Availability: NASA CASI (443) 757-5802

13. SUPPLEMENTARY NOTES

14. ABSTRACT

A multiscale modeling methodology is developed for structurally-graded material microstructures. Molecular dynamic (MD) simulations are performed at the nanoscale to determine fundamental failure mechanisms and quantify material constitutive parameters. These parameters are used to calibrate material processes at the mesoscale using discrete dislocation dynamics (DD). Different grain boundary interactions with dislocations are analyzed using DD to predict grain-size dependent stress-strain behavior. These relationships are mapped into crystal plasticity (CP) parameters to develop a computationally efficient finite element-based DD/CP model for continuum-level simulations and complete the multiscale analysis by predicting the behavior of macroscopic physical specimens. The present analysis is focused on simulating the behavior of a graded microstructure in which grain sizes are on the order of nanometers in the exterior region and transition to larger, multi-micron size in the interior domain. This microstructural configuration has been shown to offer improved mechanical properties over homogeneous coarse-grained materials by increasing yield stress while maintaining ductility. Various mesoscopic polycrystal models of structurally-graded microstructures are generated, analyzed and used as a benchmark for comparison between multiscale DD/CP model and DD predictions. A final series of simulations utilize the DD/CP analysis method exclusively to study macroscopic models that cannot be analyzed by MD or DD methods alone due to the model size.

15. SUBJECT TERMS

Crystal plasticity; Dislocation dynamics; Graded material microstructure; Molecular dynamics; Multiscale analysis

16. SECURITY CLASSIFICATION OF:			17. LIMITATION OF ABSTRACT	18. NUMBER OF PAGES	19a. NAME OF RESPONSIBLE PERSON
a. REPORT	b. ABSTRACT	c. THIS PAGE			STI Help Desk (email: help@sti.nasa.gov)
U	U	U	UU	52	19b. TELEPHONE NUMBER *(Include area code)* (443) 757-5802

Standard Form 298 (Rev. 8-98)
Prescribed by ANSI Std. Z39.18